

**ANALYSIS OF REACTIVE OXYGEN SPECIES  
KINETICS IN PATHOGENIC FUNGI OF BARLEY AND MAIZE  
USING THE HYPER SENSOR**

by

Timothy Chaya

A thesis submitted to the Faculty of the University of Delaware in partial fulfillment  
of the requirements for the degree of Master of Science in Plant and Soil Sciences

Summer 2019

© 2019 Timothy Chaya  
All Rights Reserved

**ANALYSIS OF REACTIVE OXYGEN SPECIES  
KINETICS IN PATHOGENIC FUNGI OF BARLEY AND MAIZE  
USING THE HYPER SENSOR**

by

Timothy Chaya

Approved: \_\_\_\_\_  
Jeffrey L. Caplan, Ph.D.  
Professor in charge of thesis on behalf of the Advisory Committee

Approved: \_\_\_\_\_  
Nicole M. Donofrio, Ph.D.  
Professor in charge of thesis on behalf of the Advisory Committee

Approved: \_\_\_\_\_  
Benjamin Horwitz, Ph.D.  
Professor in charge of thesis on behalf of the Advisory Committee

Approved: \_\_\_\_\_  
Erik Ervin, Ph.D.  
Chair of the Department of Plant and Soil Sciences

Approved: \_\_\_\_\_  
Mark Rieger, Ph.D.  
Dean of the College of Natural and Agricultural Resources

Approved: \_\_\_\_\_  
Douglas J. Doren, Ph.D.  
Interim Vice Provost for Graduate and Professional Education and Dean  
of the Graduate College

## ACKNOWLEDGMENTS

I would like to start off by acknowledging my family. My mother Patricia, my other brother Nicholas and my younger sister Gabrielle. My mother has always pushed me, partially because I needed it, but she also saw my potential from the very beginning. Nick and Gab have been constant sources of love, absurd texts and conversations that helped me get through long hours in the lab. Equally important, my wife Melanie. Her love over the entirety of our relationship has been the motivation that I needed to get through the worst of days. She has been my constant cheerleader during my whole career.

When thinking about my career, I have had the privilege to work with many amazing people. I would like to thank the members of my first real lab job at The University of Pennsylvania: Lorenza Moronetti, Dr. Predrag Krajacic, Dr. Elizabeth Morton and Dr. Todd Lamitina. They all helped shape my first academic research lab experience over a decade ago and where I developed fundamental skills that I will use for the rest of my career. I would separately like to thank Dr. Jessica Tanis. She has played a profound role in my success since starting in Todd's lab, and I don't think I would be where I am without her encouragement and wisdom.

At the Delaware Biotechnology Institute, I would like to thank Jean Ross, Shannon Modla, Debbie Powell, Dr. Chandran Sabanayagam, and Dr. Sylvain Le Marchand. They have been vital resources for all things microscopy, science and general fun around BioImaging. I would also like to thank Dr. Mary Boggs for her excitement for science, and to Adele Paoli, Tracy Walsh and Roula Pappoulis for keeping DBI running.

I would like to thank the Caplan, Donofrio, Bais and Sherrier lab members Dr. Kun Huang, Alex Nedo, Kody Seward, Dr. Terry Mhora, Jessica Pancake, Danielle

Mikolajewski, Jonathan Neifert, Nicholas Johnson, Victoria Gundlah, Nicole Holland and Sarah Blizzard for their feedback and assistance on my project; plus listening to countless practice talks.

Lastly, my committee: my co-advisors Dr. Jeff Caplan and Dr. Nicole Donofrio, plus Dr. Ben Horwitz and Dr. Randy Wisser. I have been extremely fortunate to have a committee of wonderful people. Jeff for his seemingly infinite patience and microscopy knowledge, Nicole for her *Magnaporthe* wisdom, Ben for being on the other side of the world and still helping guide my project. Lastly, while Randy is no longer officially on my committee, I would not have come down to UD if it were not for DrMaize and his collaboration with Jeff. You have all been a pleasure to work with and learn from. I look forward to many future projects and collaborations.

## TABLE OF CONTENTS

LIST OF TABLES .....	viii
LIST OF FIGURES .....	ix
ABSTRACT .....	xiii

### Chapter

1	TWO ASCOMYCETES LIVING TWO DIFFERENT LIFESTYLES.....	1
1.1	Fungal impact on global food security .....	1
1.2	<i>Magnaporthe oryzae</i> life cycle and infection strategy .....	2
1.3	<i>Cochliobolus heterostrophus</i> life cycle and disease progression .....	4
1.4	Plant innate immunity.....	6
1.5	Reactive oxygen species- sources and detoxification .....	7
1.5.1	Superoxide anion .....	9
1.5.2	Singlet oxygen .....	9
1.5.3	Hydroxyl radical .....	10
1.5.4	Hydrogen peroxide .....	11
1.6	Comparison of <i>M. oryzae</i> and <i>C. heterostrophus</i> ROS production and detox mechanisms .....	13
1.7	Methods for detection of ROS: stains versus encoded biological indicators .....	14
1.8	Goal of the research in this thesis.....	17
2	MATERIALS AND METHODS .....	18
2.1	Barley and maize growth.....	18
2.2	<i>M. oryzae</i> culturing and spore isolation .....	18
2.3	Adjusting spore concentration for assays .....	18
2.4	<i>C. heterostrophus</i> culturing, transformation and spore isolation .....	19
2.5	<i>M. oryzae</i> and <i>C. heterostrophus</i> HyPer sensor <i>in vitro</i> perfusion assay. ....	20
2.6	ThermoFisher CX7 high content imaging of <i>M. oryzae</i> conidia.....	22
2.7	HyPer sensor activity during barley leaf pathogenesis.....	24
2.7.1	HyPer sensor levels during maize leaf pathogenesis.....	25
2.8	<i>In planta</i> live-cell imaging to capture the HyPer sensor response .....	26
2.9	Volumetric Imaging and rendering <i>M. oryzae</i> infection cycle.....	27
3	RESULTS.....	31

3.1	<i>M. oryzae</i> ROS measurement during early stages of the infection cycle	31
3.2	Creating a full 3 dimensional infection life cycle for <i>M. oryzae</i> on lacey barley.....	33
3.3	<i>C. heterostrophus</i> :HyPer inoculation of maize leaves .....	34
3.4	Perfusion assays to show ROS response kinetics in <i>M. oryzae</i> and <i>C. heterostrophus</i> .....	36
3.5	High throughput assay development for <i>M. oryzae</i> mutant screening ....	45
4	DISCUSSION.....	47
4.1	Analysis of fungal HyPer sensor kinetics in an <i>in vitro</i> environment.....	47
4.2	<i>In vitro</i> ROS kinetics for MoHyPer and <i>C. heterostrophus</i> :HyPer.....	48
4.3	<i>In vitro</i> analysis of ROS kinetics using open perfusion system. ....	49
4.4	Conclusions .....	52
	REFERENCES.....	54
Appendix		
A	FIJI DATA PROCESSING FOR 36 AND 48 HPI MOHYPER BARLEY INFECTION.....	60
A.1	Code used for FIJI processing of MoHyPer barley infection data.....	60

## LIST OF TABLES

<b>Table 1</b>	<b>Types of ROS</b> (Adapted from Wahid 2014 & Huang 2012) [28, 29] ..... 8
----------------	-----------------------------------------------------------------------------

## LIST OF FIGURES

<b>Figure 1</b>	The life cycle of <i>M. oryzae</i> . Beginning with conidiation in the center, the conidium can take one of three paths. Either asexual, sexual or entering the infection cycle. Figure from Perez-Nadales Fungal Genetics and Biology 2014.[7].....	3
<b>Figure 2</b>	<i>C. heterostrophus</i> life and disease cycle showing the two possible portions of the cycle that germinating conidia can go through. Life cycle from Yoder 1988 [20] .....	5
<b>Figure 3</b>	Eq. 1) The breakdown of $H_2O_2$ by Fe(II) is initiated by the Fenton reaction, generating a hydroxyl radical and a hydroxide. Eq. 2) The hydroxyl radical reacts again to form water, an oxygen ion and a hydrogen ion. Eq 3) Fe(III) loses an electron to the oxygen ion, creating Fe(II) and oxygen. Eq 4) The oxygen ion can react with $H_2O_2$ that has not been previously catalyzed with Fe(III) to produces molecular oxygen, a hydroxyl radical and a hydroxide. Equations from Liochev 2002 [36] .....	10
<b>Figure 4</b>	Reaction of catalase with $H_2O_2$ to form $O_2$ and $H_2O$ . [43].....	12
<b>Figure 5</b>	The reduction of $H_2O_2$ via enzymatic catalysis with ascorbate, ascorbate peroxidase, glutathione and glutathione peroxidase. Figure from Apel and Hirt 2004. [38].....	13
<b>Figure 6</b>	Upper panel showing the workflow for spore collection, filtering, concentration adjustment and plating on 22 X 22 coverglass. The lower panel is the setup of the gravity perfusion connected to the ValveBank controller. Tubing flows the solution down, across the spores on the slide and is aspirated by the MasterFlex CL variable pump.....	21
<b>Figure 7</b>	Workflow for CX7 high-throughput ROS assay. Spores from plates are isolated by filtration through 2 layers of sterile 22-25 $\mu m$ miracloth, the concentration is adjusted with a hemocytometer, and 200 $\mu l$ is plated into an IBIDI $\mu$ -bottom 96-well plate. The spores are allowed to adhere to the bottom for 30 min in the dark at room temperature. Then the plate is loaded into the CX7 and the program titled “Magnaporthe ROS assay” is run. ....	23

<b>Figure 8</b>	The CX7 automatically quantifies the image data based on parameters that are determined based of a preliminary image. The raw image is taken, and all the objects in the field are identified. Then based off of size and location anything that is above or below a certain size or on the edge of the field are excluded. Selected objects are masked, and channel 1 is quantified for a ring that encircles the entire object, and channel 2 is quantified via a spot that fills in the ring.....	24
<b>Figure 9</b>	Barley detached leaf assay at 72 HPI. Note distinct lesions where inoculation droplets were placed. ....	25
<b>Figure 10</b>	The first true leaves of B73 in 15 cm petri plate, image taken at 6 HPI.	26
<b>Figure 11</b>	The volumetric rendering of a <i>M. oryzae</i> infection site in barley, 72 HPI. XY, YZ and ZX show single slices from the volumetric dataset. The leaf tissue is shown in cyan; the infection is in red and autofluorescence in the leaf is in yellow. The upper right image shows the fully rendered image in Amira, where the leaf is in green and the hyphae is in pink.....	30
<b>Figure 12</b>	Quantification of MoHyPer during early stages of pathogenesis in the spores.....	31
<b>Figure 13</b>	Quantification of appressorial MoHyPer intensity over early infection stages. ....	32
<b>Figure 14</b>	Selected infection sites, showing a range of MoHyPer intensities at 36 and 48 HPI. The images were generated in FIJI and displayed as the 16 color LUT and scale bars are 10 $\mu$ m. ....	33
<b>Figure 15</b>	3D renderings of only MoHyPer's infection cycle on lacey barley. Leaf tissue shown in green and fungi shown in cyan. Starting with conidia released from a conidiophore, landing on a leaf's surface. 2 hours post inoculation, germ tubes from the spores are clearly visible. At 5 HPI, early appressoria form, and when 22-24 HPI are reached, <i>M. oryzae</i> forms a penetration peg and enters the epidermal cell. At 36 HPI the bulbous hyphae have filled the initial infected cell. 48 and 72 HPI the fungus moves through the leaf tissue and exits. Upon exiting, conidiation will occur and the infection cycle can start over. Inoculated leaf tissue cleared with ScaleP protocol and imaged on Zeiss LSM880 Coherent Chameleon Multiphoton Ti:Sapphire laser tuned to 745 nm with a 40X C-Apochromat (NA 1.2) water immersion lens. Images rendered in Amira 6.3.....	34

<b>Figure 16</b>	A comparison of <i>C. heterostrophus</i> WT C4 and HyPer expressing lines, 2 HPI on B73 maize first leaves. Upper panels showing lack of fluorescence when compared to the ratiometric output of the HyPer sensor at the same time point. ....	35
<b>Figure 17</b>	6 HPI of <i>C. heterostrophus</i> :HyPer on B73 and Mo17 maize lines. Notice that in the upper panel the fungus has made an appressoria and penetrated into B73, while at a similar time on Mo17, there is only an appressoria formed. ....	36
<b>Figure 18</b>	<b>A.</b> Cropped spore in DIC and ratiometric intensity between 488:405 nm excitation. <b>B-F</b> Differences in response to varied concentrations of H <sub>2</sub> O <sub>2</sub> being flowed through the imaging chamber. Each curve is representative of different spores imaged. Sterile water (blue), 1 mM DTT (yellow) and 10mM H <sub>2</sub> O <sub>2</sub> (pink). Error bars = SD.....	37
<b>Figure 19</b>	Perfusion response curve for MoHyPer showing response to sterile water(blue), 1 mM DTT (yellow) and 10 mM H <sub>2</sub> O <sub>2</sub> (pink). Image channel intensity quantified in FIJI and graphed in GraphPad Prism. Spore image processed in Zen. Level of response displayed with rainbow LUT where blue = low and red=high. Scalebar = 10 μm. ....	38
<b>Figure 20</b>	Perfusion response curve for <i>C. heterostrophus</i> :HyPer showing change in HyPer response to sterile water (blue), 1 mM DTT (yellow) and 10 mM H <sub>2</sub> O <sub>2</sub> (pink). Image channel intensity quantified in FIJI and graphed in GraphPad Prism. Spore image processed in Zen. Level of response displayed with rainbow LUT where blue = low and red=high. Scalebar = 10 μm. ....	39
<b>Figure 21</b>	The same <i>M. oryzae</i> conidia were stimulated three times with 25 mM H <sub>2</sub> O <sub>2</sub> . Sustained level of MoHyPer response begins to diminish with the second treatment of H <sub>2</sub> O <sub>2</sub> . Sterile water (blue), 1 mM DTT (yellow) and 10 mM H <sub>2</sub> O <sub>2</sub> (pink). ....	40
<b>Figure 22</b>	A mixed population of <i>C. heterostrophus</i> :HyPer sensor conidia with two repeated stimulations of 10 mM H <sub>2</sub> O <sub>2</sub> .....	41
<b>Figure 23</b>	Perfusion assay of MoHyPer with 140 μM menadione. Sterile water(blue), 1 mM DTT (yellow) and 140 μM Menadione in 95% EtOH (red). ....	42
<b>Figure 24</b>	Perfusion assay of menadione sodium bisulfite (MBS). A - C 140 μM, 1 mM and 10 mM MBS respectively. Sterile water(blue), 1 mM DTT (yellow) and 10 mM H <sub>2</sub> O <sub>2</sub> (pink). ....	43

<b>Figure 25</b>	Perfusion assay showing the sensitivity of MoHyPer in response to pH extremes. Response is significant. p-value <0.001 .....	44
<b>Figure 26</b>	<i>C. heterostrophus</i> :HyPer single conidia treated with 1 X PBS buffers of different pH concentrations.....	45
<b>Figure 27</b>	<i>M. oryza</i> spores plated in quadruplicate were imaged three times over an hour to measure the consistency of HyPer response over an extended period. Error bars = SD .....	46

## ABSTRACT

*Magnaporthe oryzae* and *Cochliobolus heterostrophus* represent two important fungal pathogens that pose a threat to global food production. The hemi-biotroph *M. oryzae* has a broad host range with the ability to infect rice, barley, millet, and other grasses. *C. heterostrophus* on the other hand is a necrotroph with a host range of maize, soybeans, millet, wheat and teosinte. The fungal infection in host plant tissue is a complex process that is in part defined by regulation of Reactive Oxygen Species (ROS). It is well established that plants use ROS as a key component of innate immunity, growth and development. Analogously, fungi need ROS for development and production of necessary infection structures. In both organisms, ROS production must be carefully regulated to prevent deleterious effects. This research is exploring the ROS dynamics in both fungal systems. It is hypothesized that these pathogens will utilize and regulate ROS in a different manner during infection.

To aid in the understanding of this process, I am utilizing a genetically encoded reporter for hydrogen peroxide called HyPer. Three different microscopy approaches for ROS kinetics were conducted. The first was an *in-situ* analysis of conidia in a perfusion chamber, characterizing the response kinetics of each fungus when treated with oxidative (hydrogen peroxide) or reductive (dithiothreitol) solutions. The second approach was imaging *in planta* ROS levels through select infection stages. The last approach was the generation of a high throughput imaging workflow to analyze HyPer sensor mutants in future forward genetic screens. With a baseline of how each fungus responds to ROS, we plan to analyze HyPer mutant libraries under development for forward genetic screens, to identify genes related to ROS generation and attenuation.

These genes can provide targets for the development of new fungicides or breeding of more resistant plants.

## Chapter 1

### TWO ASCOMYCETES LIVING TWO DIFFERENT LIFESTYLES

#### 1.1 Fungal impact on global food security

Currently fungal pathogens pose a considerable threat to global food production. The Food and Agriculture Organization calculates that 48.1% of the modern diet is composed of five major crops. Of these five, rice and maize make up a significant portion at 18.9 and 5.4% respectively. [1] It is also estimated that 22.5% of maize and 30% of rice is lost to pests and pathogens globally. Two important fungal pathogens of these crops are the hemi-biotroph *Magnaporthe oryzae* (rice) and necrotroph *Cochliobolus heterostrophus* (maize). The major impact of these fungi is felt in areas that already struggle with food availability and have an increasing population. [2] To meet our food demands by 2050, it is projected that we will need to increase food production by 60%. [3] One important way to meet this demand is to prevent loss of crops to disease. Through selective application of fungicides, crop management and breeding this can be accomplished. For these strategies to be effective however, we must first understand the biology of how these fungi invade their hosts and carry out their life cycles.

A key component of this interaction is the production of Reactive Oxygen Species (ROS). Both the plant host and the fungal pathogen produce and detoxify ROS because it is a by-product of respiration in the environment. For the scope of this thesis, I will first cover the life cycles for both pathosystems, plant innate immunity, production

and regulation of ROS within plants and then discuss what is known for the analogous mechanisms in *M. oryzae* and *C. heterostrophus*.

## **1.2 *Magnaporthe oryzae* life cycle and infection strategy**

*M. oryzae* is a filamentous ascomycete that lives a hemibiotrophic lifestyle. The infection range for *M. oryzae* include rice (*Oryzae sativa*), foxtail millet (*Setaria italica*), finger millet (*Eleusine coracana*), wheat (*Triticum aestivum*), and oat (*Avena sativa*). [4] The lifecycle, shown in Figure 1, has three branches that a conidium can go through. For the purposes of this thesis, I will only be focusing on the portion of the infection portion of the life cycle. To begin, conidia are released from conidiophores and are dispersed through the air via wind or water droplets and land on the surface of the host plant with potential to infect all parts and growth stages. [5] The three celled spore senses and adhere to the hydrophobic leaf surface with a complex of sugar, neutral lipids, and hydrophilic amino acids. [6] Once adhered, the conidium extend out a polarized germ tube which will then form a bulbous structure called an appressorium.

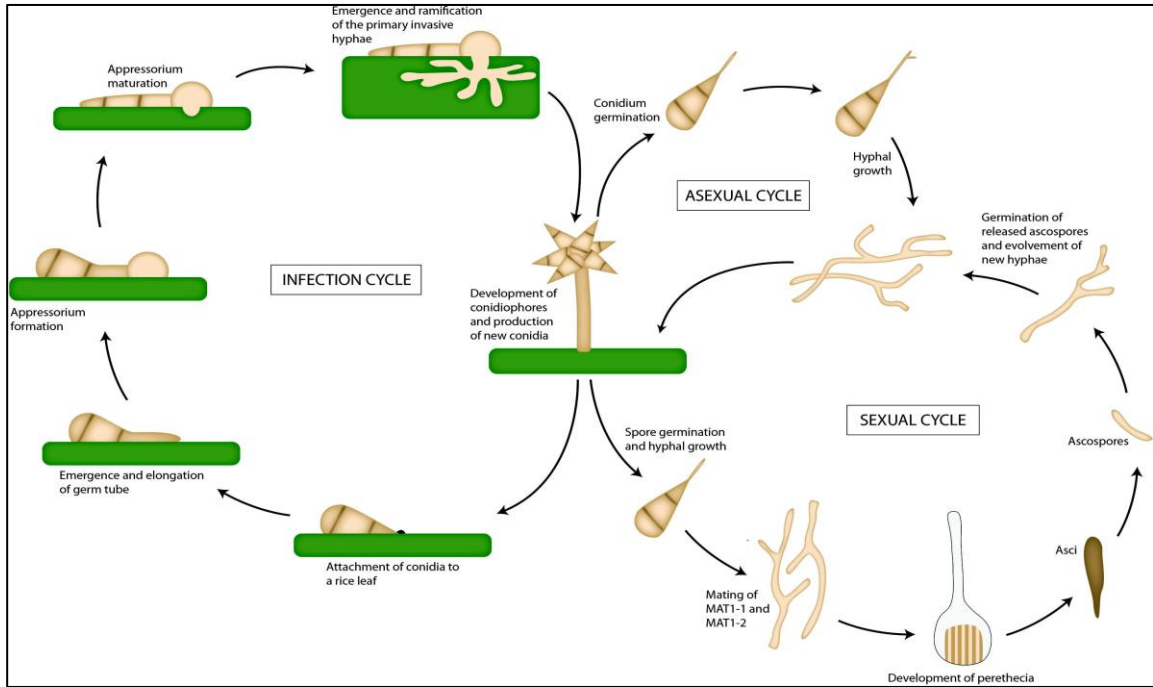


**Figure 1** The life cycle of *M. oryzae*. Beginning with conidiation in the center, the conidium can take one of three paths. Either asexual, sexual or entering the infection cycle. Figure from Perez-Nadales Fungal Genetics and Biology 2014.[7]

This dome-shaped structure becomes melanized and through the production of high amounts of glycerol, it generates a force of 8 MPa. This force is directed through the cuticle of the leaf forming a penetration peg. [8] The localization of this penetration peg is directed by the reorganization of the filamentous (F)-actin cytoskeletal network. This reorganization is assisted by NADPH oxidases Nox1, Nox2 and NoxR. [9] Deletions of these NOX genes inhibit the ability of the appressoria to infect. [8] When entering the host tissue, *M. oryzae* does an exceptional job at evading the host response by remaining coated in the plant-derived extrinsic hyphal membrane (EIHM). [10] With this cloaking mechanism, it forms a Biotrophic Interfacial Complex (BIC) which serves as

a site of production and excretion of effectors into the cytosol and apoplast. Effectors that modulate plant host resistance are called Avirulence proteins (*AVR*) have been extensively studied in *M. oryzae*. *AVR-Pitz*, *AVR-Pita*, *PWL1* and *PWL2* are secreted from the BIC into the cytoplasm [10]. Apoplastic effectors, like *Bas4*, *Bas13* and *Slp1*, are retained in the apoplast. It is unclear what sequence or structural elements determine if an effector is cytosolic or apoplastic. [11] These molecules serve to alter the host cells and suppress the defense response. [10] The initially infected cell then becomes full of bulbous invasive hyphae that are searching out plasmodesmata. The hyphae then constrict from 5.0  $\mu\text{m}$  to 0.6  $\mu\text{m}$  to enter the neighboring cell. This invasive growth to the next cell is regulated by a fungal mitogen-activated protein kinase called *Pmk1*. [12] As the fungus spreads to the surrounding tissue, necrotic lesions will form, and *M. oryzae* will begin sporulation to continue the infection cycle.

### **1.3 *Cochliobolus heterostrophus* life cycle and disease progression**

The ascomycete *C. heterostrophus* is a necrotrophic, filamentous maize pathogen in the class dothideomycete. [13] *C. heterostrophus* is the sexual stage of the anamorph *Bipolaris maydis* and causes Southern Corn Leaf Blight (SCLB). This disease was first seen in 1923 and described by Drechsler in 1925 on leaves from Florida and the Philippines that were presenting large, brown lesions from 0.5 mm to 15 mm. [14] There are three races of this pathogen present globally: Race T, Race O and Race C. Race T, the causal agent of the 1970 SCLB epidemic in the US, produces host specific toxins that are highly virulent on Texas cytoplasmic male sterile corn (*cms-T* or *T-cytoplasm*). This family of linear polyketides interact with the *cms-T* maize mitochondria in all tissues of the plant and lead to death. [15, 16] Race O on the other hand, produces toxin but it is not specific to the cytoplasm. [17] In 1988 a third race was

discovered in China called Race-C. This race also produces toxins, however they target membranes rather than the mitochondria. [18]

For all three races the pathogenicity is similar. Conidiophores are released from overwintering material, or other infected plants, and can take one of two paths shown in Figure 2. In the first option, the conidia germinate and interact with an opposite mating type. This sexual reproduction will generate the formation of pseudothecia, which contain asci full of ascospores. The ascospores can then be released into the environment to infect surrounding tissues. The second path *C. heterostrophus* can enter the leaf tissue through stomates, wounds or with appressoria. When not entering through the stomates, a weakly melanized appressoria is formed and the fungus produces cell wall-degrading enzymes. [19]

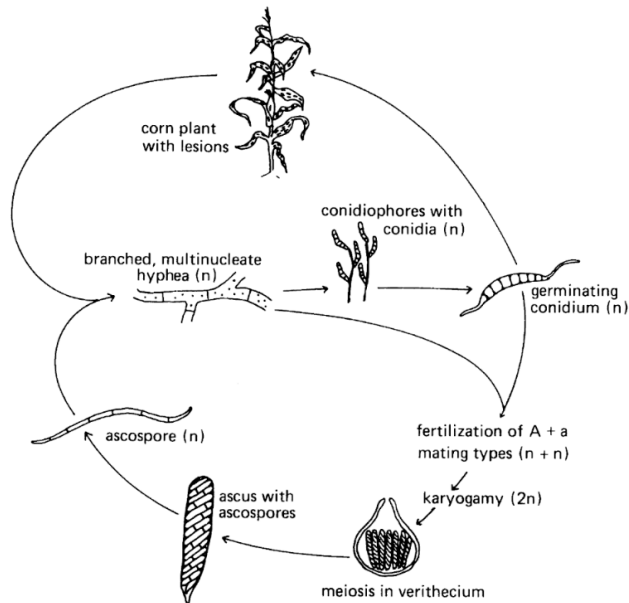


**Figure 2** *C. heterostrophus* life and disease cycle showing the two possible portions of the cycle that germinating conidia can go through. Life cycle from Yoder 1988 [20]

*C. heterostrophus* is a necrotroph that rapidly kills the host tissue, resulting in a highly oxidative environment. This oxidative environment is a product of the plant innate immunity and the response of the host protecting itself from invasion.

#### **1.4 Plant innate immunity**

Plant defense against pathogens (bacteria, viruses, fungi, oomycetes, other parasitic plants, insects) is dependent on innate immunity. Unlike a mammalian immune system, which relies on specific cells that exist within the organism to prevent disease, each cell in a plant possesses the ability to respond to disease. This defense system is separated into two branches; one is rapid and the other is a more sustained response. The rapid response is triggered by external cell surface factors on the pathogen called Pathogen Associated Molecular Patterns (PAMPs), which activate pattern-recognition receptors (PRRs) and trigger PAMP triggered immunity (PTI) (REF). The PRR's are only known to be on the surface of the cells and are receptor kinases (RKs) or receptor-like proteins (RLPs). [21, 22] PTI is a robust response to PAMPs that are conserved across phylogenetic classifications like flagellin or chitin. It is hypothesized that the RLKs have a ligand binding ectodomain which are a single-pass transmembrane domain, that leads to an intracellular kinase domain. RLPs are similar except there is no intracellular kinase domain. [22] This broad-spectrum response provides resistance to all non-adapted pathogens.

Microbes can enter the host tissue through a variety of mechanisms: bacteria can dock externally and inject effectors with Type III secretion system (TTSS), oomycetes use haustoria and fungi enter with invasive hyphae. Once the pathogen enters the host, many of these secreted effectors attenuate PTI, initiating effector triggered susceptibility (ETS). [23] It has been shown that with the TTSS, bacteria can inject up to 30 effectors

into the host cells. This interferes with cellular functions and creates a hospitable environment.[23] These secreted effectors interact directly or indirectly with R-proteins, of which a major class are nucleotide binding leucine rich repeats (NB-LRRs). These NB-LRRs have two common N-terminal domains, either a Toll/interleukin-1 receptor (TIR) or a coiled-coil (CC) domain. The identified effectors called avirulence (AVR) proteins are specific to each pathogen, and have minimal conservation at the family level. [24] The response from ETI is slower but more robust than PTI, which results in the hypersensitive response (HR), triggering cell death and limiting the spread of the pathogen. Along with triggering the HR at the local level, cell permeable immune signals travel through the surrounding tissues to increase expression of pathogenesis-related (PR) proteins. These signals cause an increase in salicylic acid (SA) which is a key inducer of systemic acquired resistance (SAR) and serve to protect the host from a broad range of future microbial invaders including viruses, bacteria, oomycetes and fungi. [24, 25] In *Arabidopsis thaliana*, SAR causes transcriptional changes of 10% of the genes in the genome. [26] A gatekeeper of SAR activity is the transcription factor NPR-1 (nonexpressor of pathogenesis-related genes 1), which when mutated results in a larger, more chlorotic lesions. [26] Through the co-evolution of plants and pathogens, it has been a proverbial arms race to evolve effectors and resistance genes. A key component of PTI and ETI is the oxidative burst that is not at a level to be antimicrobial, but acting as a mechanism to fortify cell walls, and signal to surrounding cells. [27]

### **1.5 Reactive oxygen species- sources and detoxification**

ROS have been an important biological molecule since early photosynthetic organisms have been generating molecular oxygen (O<sub>2</sub>). In response to biotic and

abiotic stress, plants can create four different types of ROS from multiple sources, with varying concentrations and degrees of toxicity. (Table 1)

**Table 1** Types of ROS (Table adapted from Wahid 2014 and Huang 2012) [28, 29]

<b>ROS</b>	<b>Makeup</b>	<b>Half-life (s)</b>	<b>Effective Distance</b>	<b>Source(s)</b>	<b>Detoxification</b>	<b>Reactivity</b>
<b>Superoxide anion</b>	$O_2^-$	$10^{-6}$	30 nm	Mitochondria, Mehler reaction in chloroplasts, Peroxisomes, NADPH Peroxidases, RBOHs, Oxalate oxidases	SOD, flavonoids and carotenoids [30]	Highly reactive with most biomolecules
<b>Hydrogen peroxide</b>	$H_2O_2$	$10^{-3}$	1 $\mu$ m	Mitochondria, Chloroplasts, Peroxisomes, NADPH Peroxidases, RBOHs, Oxalate oxidases	APX, Catalase, GPX, PrxR	Thiol groups of enzymes, $\beta$ -oxidation of membrane lipids
<b>Hydroxyl radical</b>	OH-	$10^{-9}$	1 nm	Cell wall bound peroxidase, Thylakoid membranes	Lipid peroxidation, inhibition of Haber-Weiss reaction, flavonoid scavenging[30]	Highly reactive with most biomolecules
<b>Singlet oxygen</b>	$^1O_2$	$10^{-5}$	30 nm	Chloroplast Photosystem I and PSII	Chloroplast associated carotenoids, ascorbic acid, $\alpha$ -tocopherol, secondary metabolites and quinones	Oxidizes proteins, lipids and DNA

### 1.5.1 Superoxide anion

O<sub>2</sub> is unreactive in a ground state but can be activated to form singlet oxygen (<sup>1</sup>O<sub>2</sub>) or reduced to form an extremely reactive superoxide anion (O<sub>2</sub><sup>-</sup>). This molecule has a limited lifespan and is readily produced during respiration by NADPH oxidases[31]. Estimates are that 1 out of every 2,000 electrons transferred to NADH result in the production of O<sub>2</sub><sup>-</sup>. Superoxide dismutase is the main enzyme that catalyzes the conversion of O<sub>2</sub><sup>-</sup> + O<sub>2</sub><sup>-</sup> + 2H<sup>+</sup> → H<sub>2</sub>O<sub>2</sub> and O<sub>2</sub>. The less reactive hydrogen peroxide is further reduced to water via either catalase (CAT), by taking 2H<sub>2</sub>O<sub>2</sub> and converting them to 2H<sub>2</sub>O and 2O<sub>2</sub> or glutathione peroxidase (GPX), which oxidizes thiol containing glutathione (GSH) to glutathione disulfide (GSSG) [31, 32]

### 1.5.2 Singlet oxygen

Singlet oxygen (<sup>1</sup>O<sub>2</sub>) is generated through O<sub>2</sub> and the photoexcitation of chlorophyll to the triplet state. During photosynthesis light excites a singlet state chlorophyll molecule, and this energy can be released in one of three ways. Two options are transferring that energy to drive photochemistry, or through thermal dissipation. A third option occurs when too much light energy is received, and chlorophyll enters the triplet state. In this state the chlorophyll reacts with oxygen to form <sup>1</sup>O<sub>2</sub>. [33] Excessive light driven singlet oxygen generation is hypothesized to be the source of stress-induced photo-oxidation. [34] Due to the highly reactive nature of <sup>1</sup>O<sub>2</sub> it is rapidly reduced by lipid-soluble antioxidants like carotenoids and α-tocopherol. [35] Research in *Chlamydomonas reinhardtii* suggests that high intensity light induced <sup>1</sup>O<sub>2</sub> leads to the expression of a nuclear-encoded glutathione peroxidase. [33] This suggests that while

$^1\text{O}_2$  is highly reactive, it possibly escapes scavenging molecules and triggers a cascade to respond to high intensity light.

### 1.5.3 Hydroxyl radical

$\text{OH}^\cdot$  is produced following the reduction of  $\text{H}_2\text{O}_2$  in the Fenton and Haber-Weiss reaction. (Figure 3) This radical has a high oxidizing potential and is hazardous to all biological molecules.

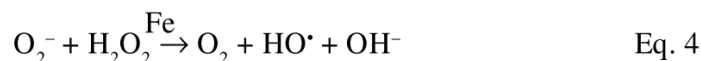
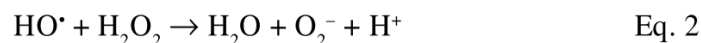


**Figure 3** Eq. 1) The breakdown of  $\text{H}_2\text{O}_2$  by  $\text{Fe(II)}$  is initiated by the Fenton reaction, generating a hydroxyl radical and an hydroxide. Eq. 2) The hydroxyl radical reacts again to form water, an oxygen ion and a hydrogen ion. Eq 3)  $\text{Fe(III)}$  loses an electron to the oxygen ion, creating  $\text{Fe(II)}$  and oxygen. Eq 4) The oxygen ion can react with  $\text{H}_2\text{O}_2$  that has not been previously catalyzed with  $\text{Fe(III)}$  to produces molecular oxygen, a hydroxyl radical and a hydroxide. Equations from Liochev 2002 [36]

However, since the hydroxyl radical is so reactive, it is generally scavenged at the site of production. It has been shown that thioredoxin, ferredoxin, glutathione and flavonoids are capable of scavenging  $\text{OH}^\cdot$ . [37]

#### 1.5.4 Hydrogen peroxide

When compared to the other ROS that have been described thus far, hydrogen peroxide,  $\text{H}_2\text{O}_2$ , has the longest half-life which makes it a suitable signaling molecule. It has variety of production sites, including the mitochondria, chloroplasts, NADPH oxidases, respiratory burst oxidase homologs (RBOHs), peroxisomes and oxalate oxidases. Plants have a limited amount of ROS that is produced from the mitochondria. This is due to an enzyme in the plant mitochondria called alternative oxidase that reduces  $\text{O}_2$  with ubiquinone. [38] Chloroplasts generate  $\text{H}_2\text{O}_2$  through the dismutation of singlet oxygen formed in Photosystem I. [39] Host plant sources of ROS that are used for pathogen defense purposes are plasma membrane NADPH oxidases and cell wall peroxidases. The NADPH oxidase is a multi-subunit enzyme, which has been well described for its role in mammalian neutrophils, but the structure and activation in plants is still poorly understood. [40] Another source of defense induced  $\text{H}_2\text{O}_2$  is pH-dependent cell-wall peroxidase. These are stimulated through a change in the concentration of  $\text{Ca}^{2+}$ ,  $\text{K}^+$ ,  $\text{H}^+$  and  $\text{Cl}^-$  ions, resulting in the alkalization of the extracellular matrix. This causes the cell-wall peroxidase to change conformation and with FeII produce  $\bullet\text{O}_2^-$ , that is converted to  $\text{H}_2\text{O}_2$ . This oxidative burst leads to cell wall crosslinking and lignification. [41]

Like the previously mentioned ROS,  $\text{H}_2\text{O}_2$  is quenched via enzymes and non-enzymatic means to limit the potential cellular toxicity. [31] A chief enzyme for dismutation of  $\text{H}_2\text{O}_2$  to  $\text{H}_2\text{O}$  and  $\text{O}_2$  is catalase (CAT). Both plants and fungi carry CAT genes which utilize  $\text{Fe}^{3+}$  to form an intermediate Compound I, followed by a catalytic decomposition step. This results in the conversion of  $2 \text{H}_2\text{O}_2 \rightarrow \text{O}_2 + 2 \text{H}_2\text{O}$ . Notably, catalase does not require a cofactor or reductant to facilitate the dismutation reaction, and is reliant on a heme within the enzyme. [42]

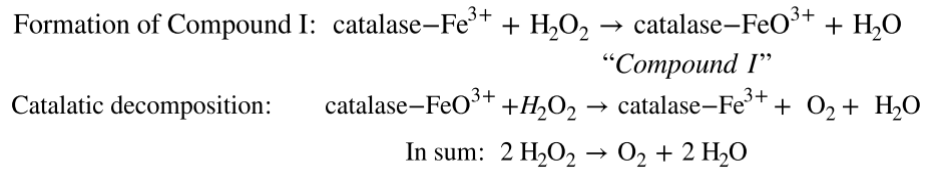


**Figure 4** Reaction of catalase with H<sub>2</sub>O<sub>2</sub> to form O<sub>2</sub> and H<sub>2</sub>O. [43]

Similarly, ascorbate peroxidase (APX) relies on a heme group, however it is also dependent on ascorbate to catalyze the detoxification of H<sub>2</sub>O<sub>2</sub>. There is a diverse array of APX isoforms that are categorized based on cellular localization, and expression is increased under various environmental stresses. [44] Glutathione peroxidase (GPX) utilizes glutathione (GSH) pools, however GPX is a non-heme containing enzyme. GSH and ascorbate work together (Figure 5) in a cycle where ascorbate and H<sub>2</sub>O<sub>2</sub> are catalyzed by APX to form water and monodehydroascorbate (MDA). The MDA and NADPH are converted to ascorbate and NADP<sup>+</sup> by monodehydroascorbate reductase (MDAR). MDA can also spontaneously produce dehydroascorbate, which in the presence of GSH is catalyzed by DHA reductase (DHAR) to form ascorbate and oxidized glutathione (GSSG). The cycle is completed by the catalysis of GSSG and NADPH by glutathione reductase (GR) to GSH and NADP<sup>+</sup>. [38]

#### Ascorbate-Glutathione Cycle:

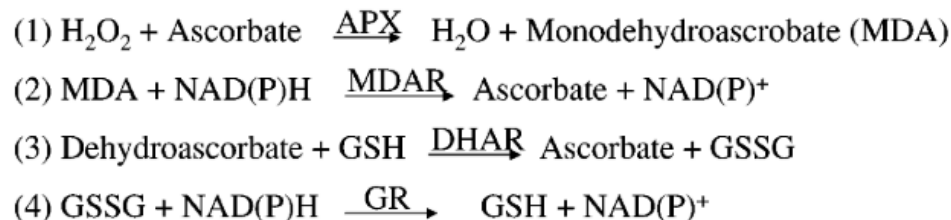


**Figure 5** The reduction of  $\text{H}_2\text{O}_2$  via enzymatic catalysis with ascorbate, ascorbate peroxidase, glutathione and glutathione peroxidase. Figure from Apel and Hirt 2004. [38]

### 1.6 Comparison of *M. oryzae* and *C. heterostrophus* ROS production and detox mechanisms

During the growth and infection cycle both pathogens are producing and detoxifying ROS. However, the sensitivity and response of the respective fungi differs greatly. When the interaction begins, the host responds with an initial ROS burst generated from membrane-associated respiratory burst oxidative homologs (RBOHs). This burst occurs for both susceptible and resistant interactions, although when the host is susceptible to infection there is a secondary longer burst referred to as the recognition response. [27, 45, 46] For detection of this oxidative change, homologs of a heavily conserved transcription factor AP-1 (Activator Protein 1) are relied upon. The general structure of AP-1 is a basic leucine zipper (bZIP) domain, two cysteine-rich domains, carboxy terminal (c-CRD) and an amino terminal (n-CRD). During activation, intramolecular disulfide bonds form which mask the nuclear export signal, allowing AP-1 to translocate from the cytosol to the nucleus leading to the expression of oxidative response genes. [47-50] Knocking out the yeast homologue yAP-1, results in sensitization to oxidative stress. [51] Similarly in *M. oryzae*, the MoAP-1 deletion mutant is sensitized to oxidative stress. Analysis of this mutant shows that there is

normal germination and appressorial formation, however pathogenicity is reduced. [52] Similarly ChAP1, the AP1 homolog in *C. heterostrophus* translocates to the nucleus during oxidative stress, however deletion of ChAP1 does not reduce pathogenicity. [47, 53] This indicates that *C. heterostrophus* is either relying on another means of oxidative stress signal transduction or has other methods to buffer itself from damage.

Fungi possess similar antioxidant tools that plants utilize and are triggered through the activation of Yap1 or its homologues. As mentioned in the previous sections about ROS generation, SOD, GPX, APX all play a role in the detoxification of host and self-generated ROS. In *M. oryzae*, loss of these enzymes as well as Des1 (defense suppressor 1), Hyr1 (glutathione peroxidase GPx3), Gtr1 (glutathione reductase), prevent entrance of the fungi into the host due to the inability to respond to host generated ROS. Conversely, mutants of the nitronate monooxygenase (Nmo2), thioredoxin peroxidase (Tpx1), thioredoxin reductase (Trr1) and thioredoxin (Trx2), can enter the host tissue, but fail to proliferate beyond the first infected cell. [54] There are many genes left to be completely described in this response, like *M. oryzae* Des-1 (defense suppressor 1), which has unknown biochemical properties, but is necessary for detoxification of host produced ROS. [55] Many of the known oxidative response genes in *C. heterostrophus* appear to be more dispensable. Catalase for example, has three known genes in the *C. heterostrophus* genome (Cat1-3).  $\Delta$ Cat3 is the only one that experiences decreased growth in the presence of hydrogen peroxide, and knockouts of all three mutants have normal virulence. [56]

### **1.7 Methods for detection of ROS: Stains versus encoded biological indicators**

ROS are challenging molecules to capture since they are transient and produce colorless products. With current imaging technologies, ROS detection falls into one of

two categories; histochemical or fluorescent protein modification. Currently, ThermoFisher offers 34 products that can detect ROS and reactive nitrogen species (RNS). Non-fluorescent histochemical approaches include nitro blue tetrazolium (NBT) for superoxide and 3,3 -diaminobenzidine (DAB) to detect H<sub>2</sub>O<sub>2</sub>. Both stains result in a chromatic detection of their respective ROS molecules. However, their detection is on the scale of hours, which is troublesome for interpreting rapid infection response kinetics. [57] There are a multitude of fluorescent based methods which makes it possible for the detection of all ROS and RNS molecules. Common fluorescent techniques for work in planta and fungi include 2',7'-dichlorodihydrofluorescein diacetate (H<sub>2</sub>DCF-DA), CellROX, and MitoSOX. [58-60] The rate of detection for these probes is more rapid than the DAB and NBT and can be live imaged in plants. The limiting factor for these stains is rate of diffusion into the plant cells. H<sub>2</sub>DCF-DA can also be cleaved by intracellular esterases, which can confound interpreting results if proper controls are not run.

In the last 13 years, genetically encoded fluorescent redox sensors have become a popular tool for investigation of ROS dynamics. Fluorescent probe (FP) based sensors have many benefits over chemical-based detections. They have been expressed in a variety of biological systems and can be preferentially expressed in specific tissues or cells. Genetic encoding bypasses the issue of limited penetrance of chemical stains into the cellular compartments. These FP-sensors are reversible and can be repeatedly stimulated, showing the spatial and temporal dynamics of their intended targets. [61] Many of these sensors are designed with a circularly permuted FP joined to a target binding specific polypeptide. When this linker interacts with the target molecule of interest, this results in a conformational change in the FP that can be detected. This was

first demonstrated in a  $\text{Ca}^{2+}$  sensor, and similar technology have been developed to detect  $\text{NAD}^+/\text{NADPH}$ ,  $\text{ATP}/\text{ADP}$ ,  $\text{CO}$ ,  $\text{GSH}/\text{GSSG}$  and  $\text{H}_2\text{O}_2$ . [61] Within the FP detection of these molecules, there are two methods for quantification of fluorescent signal; intensometric and ratiometric. Intensometric quantification measures the intensity when excited at a specific wavelength and emission at a single peak. Ratiometric is the ratio between two fluorescent signals and can be divided into two classifications. The first excitation-ratiometric, measuring two excitations with a single emission, and the second emission-ratiometric, where a single excitation being measured at two emissions. Both methods allow for the normalization of the intensity based on the expression of the protein. For ROS detection related to the experiments in this thesis, we relied upon the HyPer Sensor, which was initially developed for use in mammalian cells, but has since been expressed in a variety plant and fungal systems. [62] The HyPer sensor is a circularly permuted YFP fused to the OxyR domain from *E. coli*. This domain was shown to be selective to only hydrogen peroxide, and when stimulated results in a disulfide bridge forming between Cys199 and Cys208. This disulfide bond is reversible, allowing for measurements to be taken throughout the lifetime of the probe within the cell. The sensor is excited with 405 and 488 nm laser and a single emission at 516 nm is taken. HyPer has been shown to be susceptible to high pH, however a ROS insensitive variant has been produced called SypHer that makes it possible to determine if changes are due to pH. [63] For *M. oryzae* research, HyPer has been codon optimized using the *Neurospora crassa* codon bias and is referred to as MoHyPer. Previous research has shown it to be a viable tool for analysis of ROS kinetics within *M. oryzae* and during infection of plant tissue. [62] The HyPer sensor

has also been expressed in *Fusarium graminearum*, and *Cochliobolus heterostrophus*. [53, 64-66]

### **1.8 Goal of the research in this thesis**

With the increasing threat to global food production brought about by fungal pathogens it is important to understand the mechanisms that drive their ability to colonize host tissue. Previous studies have shown that *M. oryzae* and *C. heterostrophus* have differing host interaction mechanisms. *M. oryzae* relies on effectors to attenuate the host immune response and alter the cellular environment to allow for proliferation in a hemi-biotrophic manner, while *C. heterostrophus* produces host specific toxins that enable its necrotrophic life style. It is understood that ROS plays a major role in communication and defense from both organisms in this interaction. Deletions in ROS sensing and detoxification genes decrease the success of *M. oryzae*'s pathogenesis but have little to no effect in *C. heterostrophus*. Our hypothesis is that *C. heterostrophus* will exhibit differing ROS dynamics that *M. oryzae* in both *in vitro* and *in planta* assays. To gain insight into this interaction, the use of the HyPer sensor will permit the analysis of real-time ROS kinetics during pathogenesis during both *in vitro* and *in planta* assays.

## Chapter 2

### MATERIALS AND METHODS

#### 2.1 Barley and maize growth

Lacey Barley from Jensen Seed Company (Stephen, MN) was planted in 15 cm pots containing Redi-Earth potting soil with 6 seeds per pot. Containers were put in a Perceval growth chamber with a daytime temp of 22 °C and a nighttime temp of 18 °C. No humidity control was used. Leaves were harvested at 5-7 days post planting and were 10-12 cm long.

B73 and Mo17 maize seeds were planted in 20 cm pots containing ProMix BX. Initial growth for inoculation experiment, pots were put in same growth chamber as barley. The first true leaves were harvested 20 days post planting.

#### 2.2 *M. oryzae* culturing and spore isolation

Filter paper stocks of *M. oryzae*, 4091 MoHyPer (MoHyPer) were started on complete media (CM) containing 25 mg/ml bialaphos. Approximately one week later, 1 cm<sup>2</sup> plugs were collected from the growing edge and transferred to oatmeal agar (OMA) containing appropriate selection.

#### 2.3 Adjusting spore concentration for assays

It is necessary to adjust the spore concentrations to be uniform across assays since not all plates, and strains produce spores equally. This was done by taking oatmeal agar plates that are 7-10 days old. The starting culture for these plates, must be under a month old and cannot be passaged more than three times. The plates are washed with roughly 3 ml of sterile milliQ water, and the spores are loosened from the surface with a sterile inoculating loop. Care was taken not to remove chunks of media and hyphal

mats, as they will clog the Miracloth. The collected spore:water mixture was then taken to the Zeiss Axioplan 2 light microscope, whereupon 10  $\mu$ l was put on a Neubauer hemocytometer, and the large boxes in the four corners plus the center were counted. Spores touching the edges of the large boxes were not counted. The average was taken for each of the boxes, and then multiplied by 2,000. The reason we sum the boxes counted and then multiply by 2,000 is to give the number of spores per 1 ml of solution. This was then adjusted as needed per assay. The perfusion and CX7 assays can tolerate a higher spore concentration since they are relatively short term, however leaf blade inoculations must be lower otherwise the hyphae will overgrow and will confound any microscopy. For leaf inoculation assays, the concentration of spores was adjusted to  $1 \times 10^2$ - $1 \times 10^3$  spores per ml. For perfusion and CX7 assays, the spore concentration was  $1 \times 10^4$  spores per ml.

#### **2.4 *C. heterostrophus* culturing, transformation and spore isolation**

*C. heterostrophus* C4 culture was received from Dr. Gillian Turgeon at Cornell University with assistance from John González. Wildtype cultures of C4 are maintained on Complete Media and used to start cultures to generate protoplasts following Dr. Turgeon's original protocol. [67] This generated  $6.75 \times 10^6$  protoplasts that were used for six different transformations, plus controls. Two different HyPer constructs were transformed; 1) HyPer inserted into an *Aspergillus* PTrpC promoter with hygromycin selection, 2) MoHyPer which has been optimized to the *Neurospora crassa* codon bias. pIGPAPA, which has been successfully transformed before by the Turgeon and Horwitz labs, was used as a positive control This is a GFP producing plasmid with Hyg selection. All plasmids were transformed separately as linear and circular because it was suggested

that some vectors integrate better when linearized pre-transformation. A protoplast only, no DNA control showed the viability of the protoplasts. After four days at 30° C successful transformations led to colonies being growing through the appropriate selective media. Small plugs from isolated colonies were transferred to CM no salts media appropriate selection to grow. A copy of the clones was left in the Turgeon lab as a backup and for potential future collaboration. The transformation of circularized HyPer resulted in 11 colonies, and the linear version resulted in one. MoHyPer transformants were very slow to grow. However, after 7 days at 30° C, three colonies grew from the circular transformation and one from the linear. The pIGPAPA circular transformation generated one colony, and the linear resulted in 23. Nine HyPer, four pIGPAPA and four MoHyPer transformations were glycerol stocked in CM containing 25% glycerol. Successful transformants were confirmed via spectral signature on LSM 710 laser scanning confocal microscope. Further single spore isolation and conformation is ongoing at the time of writing. For assays, conidia from CMX+ hyg plates were isolated by washing the plate with 3 ml sterile water and filtering the solution through two layers of autoclaved cheese cloth. This resulted in a mix of spores and hyphae and will need to be further optimized for future assays.

## **2.5 *M. oryzae* and *C. heterostrophus* HyPer sensor *in vitro* perfusion assay.**

The setup of the perfusion process is illustrated in Figure 6. Conidia, whose isolation was described in sections 2.2 and 2.3 were spotted on 22 X 22 coverglasses and kept in sealed petri plates in the dark for 2 hours. This time allowed for the conidia to put down mucilage to adhere to the coverglass. 1 mM dithiothreitol (DTT) and varied concentrations of H<sub>2</sub>O<sub>2</sub> were made in sterile water. 30% H<sub>2</sub>O<sub>2</sub> stock solution (8.8 M) from Sigma was transferred to a syringe top bottle and the air was flushed out with

nitrogen gas to prevent the  $H_2O_2$  to naturally reduce to  $H_2O$ . A single inoculated coverglass was placed in a Chamlide Live Cell perfusion chamber. Solutions were loaded into 60 ml, open syringes attached to an AutoMate Scientific ValveBank-8 II. The syringes are held on a metal stand, approximately 24 inches from the top of the bench. 1/16" o.d. tubing is used to connect the syringes, through the ValveBank to the perfusion chamber.

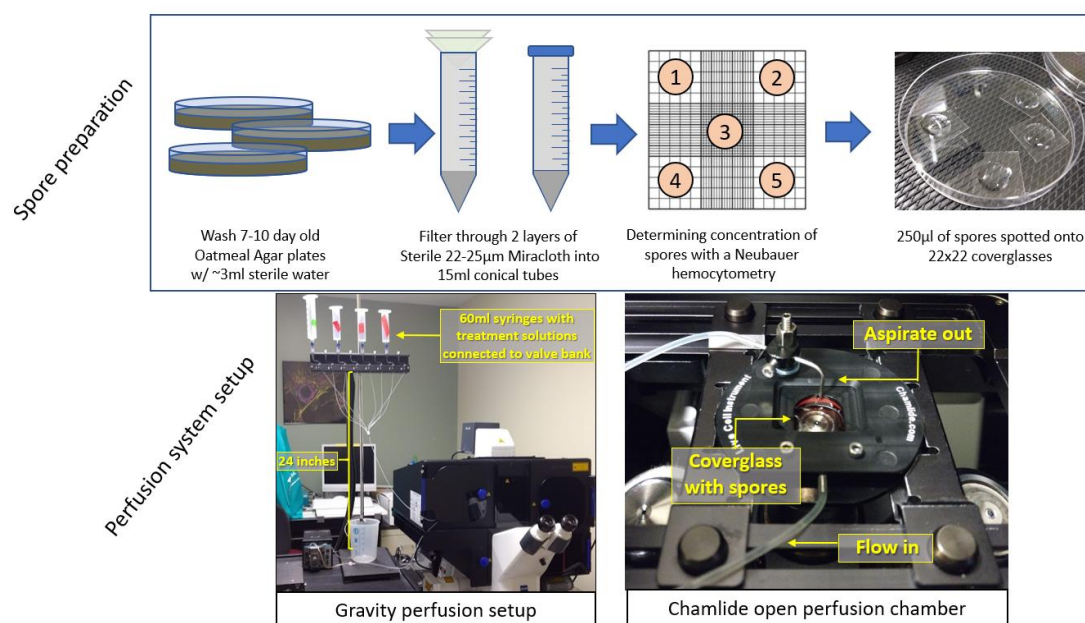


**Figure 6** Upper panel showing the workflow for spore collection, filtering, concentration adjustment and plating on 22 X 22 coverglass. The lower panel is the setup of the gravity perfusion connected to the ValveBank controller. Tubing flows the solution down, across the spores on the slide and is aspirated by the MasterFlex CL variable pump.

The solution flowed across the coverglass at a rate of 45  $\mu$ l/ second and continuously aspirated using a Cole-Parmer MasterFlex C/L variable speed pump.

Solutions are changed manually using the ValveBank control box and timing is monitored with a conventional stopwatch. The tubing connecting the ValveBank syringes to the perfusion chamber were taped to the side of the incubation chamber to reduce movement generated from the MasterFlex pump. This ensures that the movement of the tubing does not generate vibrational noise during imaging. All perfusion assays were carried out on the Zeiss LSM710 confocal microscope using the 40X Planneofluar NA1.3 oil immersion objective. The pinhole was set to 100 and the Definite Focus was set on the middle focal plane for the majority of the spores in the field. The field was autofocused and imaged every 15 seconds. In the H<sub>2</sub>O<sub>2</sub> concentration tolerance assay, a new coverglass of spores was used for 5, 10, 25, 50 and 100 mM H<sub>2</sub>O<sub>2</sub>. Intensity of response was quantified in FIJI 1.52 by drawing regions of interest within spores, and then calculating 488:405 ratio to quantify HyPer response to stimuli. [68] These data were analyzed in GraphPad 6.3.

## **2.6 ThermoFisher CX7 High content imaging of *M. oryzae* conidia**

For rapid analysis of HyPer levels in conidia in water and H<sub>2</sub>O<sub>2</sub>, a protocol for the ThermoFisher CX7 High Content imaging system has been developed, shown in Figure 7. This system will be used in a wide field illumination, where channel 1 is the blue 386 nm excitation 350 nm emission and channel 2 is 485 nm excitation, 488 nm emission. Exposure time for both channels was 0.3 seconds with a light intensity of 100%. Images were acquired with an Olympus 20X 0.7 NA air objective. Spores were isolated following the protocol from sections 2.2 were plated in Ibidi 96-well coverglass bottom  $\mu$ -plates (Catalogue number 89626) at a concentration of  $1 \times 10^4$ . This allowed for spores to be close enough that many could be captured per image field, but not overlap. The plate incubated at room temp ( $\sim 19^\circ\text{C}$ ) for 30 min. The solution was

removed from the wells and replaced with 0, 1, 10, 25 and 50 mM H<sub>2</sub>O<sub>2</sub> in quadruplicate for each sample and the plate was loaded into the CX7. The same plate was imaged at 0, 16 and 60 minutes post addition of H<sub>2</sub>O<sub>2</sub>. The 16 minute time point was based on the time it took to make the initial run. During the acquisition the CX7 analysis software counted objects based on size, which was determined during a pre-run calibration step. The object identification steps are shown in Figure 8. For each well there was a maximum of 18 wells, with a minimum of 300 objects per well, and for sparse wells a maximum of 9 fields was imaged. From these data acquired, the average intensities of channel 1 and 2 were compared as a ratio and graphed with the standard deviation.

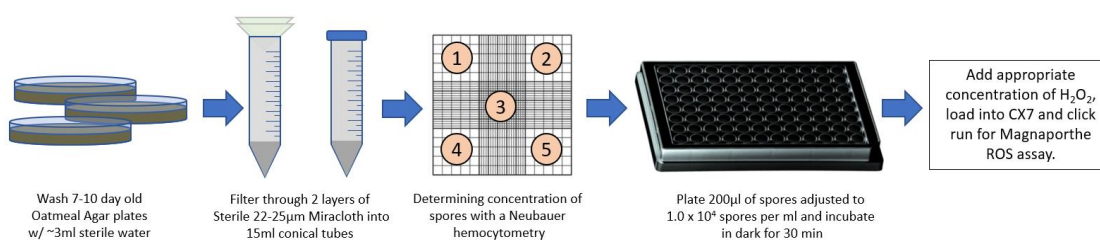


**Figure 7** Workflow for CX7 high-throughput ROS assay. Spores from plates are isolated by filtration through 2 layers of sterile 22-25 µm miracloth, the concentration is adjusted with a hemocytometer, and 200 µl is plated into an IBIDI µ-bottom 96-well plate. The spores are allowed to adhere to the bottom for 30 min in the dark at room temperature. Then the plate is loaded into the CX7 and the program titled “Magnaporthe ROS assay” is run.

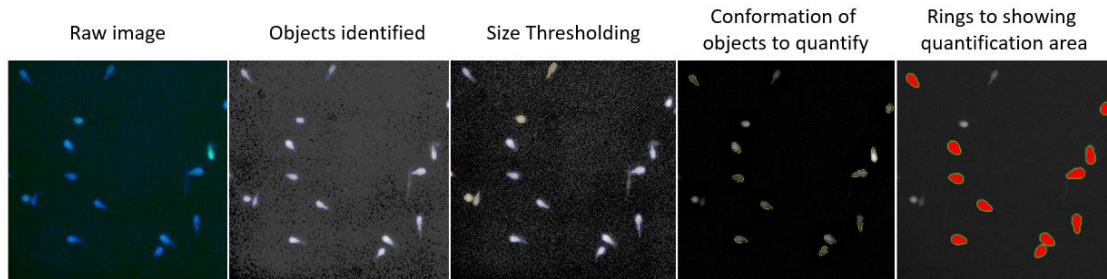


**Figure 8** The CX7 automatically quantifies the image data based on parameters that are determined based of a preliminary image. The raw image is taken, and all the objects in the field are identified. Then based off of size and location anything that is above or below a certain size or on the edge of the field are excluded. Selected objects are masked, and channel 1 is quantified for a ring that encircles the entire object, and channel 2 is quantified via a spot that fills in the ring.

## 2.7 HyPer sensor activity during barley leaf pathogenesis

Barley leaves that were described in section 2.1 were harvested 5-6 days post planting. The leaves were detached with a sterile razorblade and put on top of two moist paper towels and are taped with the adaxial side facing up in 15 cm plate. (Figure 9) The cut end of the leaf is left exposed and kept hydrated with a wet KimWipe. Leaves are inoculated with a 20  $\mu$ l of conidia at a concentration of  $1 \times 10^3$  and the plate is covered and put on top wet paper towels inside of a large 14-gallon Rubbermaid container. Temperature and humidity are maintained with three – one-liter beakers containing hot water from the tap. Leaves are kept in the dark overnight, and the following day the droplet of water is carefully removed using the edge of a KimWipe. Plates are then wrapped in plastic wrap and put in a 25°C incubator until imaged.



**Figure 9** Barley detached leaf assay at 72 HPI. Note distinct lesions where inoculation droplets were placed.

### **2.7.1 HyPer sensor levels during maize leaf pathogenesis**

20 days post germination the first true leaves of B73 and Mo17 were collected and placed in a 15 cm plate on a moist paper towel. (Figure 10) Leaves were between 8 and 10 cm. If leaves did not reach the top of the paper towel, a sterile wooden stick from a cotton swab was used to hold the leaf flat against the paper towels. 20  $\mu$ l of *C. heterostrophus*:HyPer conidia at concentration of  $1 \times 10^2$  per ml was dropped onto the leaf surface. Plates were covered and put at 25° C until ready to be imaged.



**Figure 10** The first true leaves of B73 in 15 cm petri plate, image taken at 6 HPI.

## 2.8 *In planta* live-cell imaging to capture the HyPer sensor response

The inoculated tissue that was described in previous sections was imaged on a Zeiss LSM 710 confocal microscope. They were excited with a 405 and 488 nm lasers and emission was detected between 500 and 500 nm on the Bi-GaAsP detector using a 40X PlanNeofluar 1.3 NA oil immersion objective. Areas of the inoculated leaf were cut with a single edge razor and placed spore side down in approximately 75  $\mu$ l of perfluorodecalin (Sigma 77264) in a single well, coverglass bottom Nunc™ Lab-Tek™ II Chamber Coverglass™ (Fisher 155360). Single infection sites were imaged in Z-stacks from 2-24 hours post inoculation (HPI). Five infection sites containing at least one germinated conidia were captured per leaf, before moving onto another inoculated section.

For quantification of these infection events, spores and appressoria were separately cropped in Zen Blue and then analyzed in Volocity 7.01 measuring the ratio of 488:405 (green:blue). The cropped spores or appressoria were selected via thresholding from the 488 nm green channel and then intensity was measured for both

channels. This was output as a single value for each spore wand was graphed as intensity vs. HPI.

36 and 48-hour time points were also selected to see later stages of pathogenesis, it is known that at these stages *M. oryzae* will be inside of the host tissue. The same sample inoculation and imaging settings were used as above. This data was processed in FIJI, where it was converted to 32-bit stacks, the ratio was taken between the green (channel 1) and the blue (channel 2). This ratio was then multiplied by 1000 to bring the numbers to a more usable scale and was converted to a 16 color lookup table. The brightness and contrast were equalized across all the images. The volumes were converted into maximum intensity projections (MIP) to view this complex data in a simplified manner. They were then converted back to 8-bit images and saved as a tiff file. The FIJI macro text file is in Appendix 1

## **2.9 Volumetric imaging and rendering *M. oryzae* infection cycle**

Confocal microscopy of leaf tissue is limited by the penetration of the laser into the leaf tissue and resulting scattering of light caused by lignin, cellulose, other polysaccharides as well as the convex shape of the leaf cells. For the first 25 hours of *M. oryzae*'s infection cycle on barley, it was possible to capture the spore germination, penetration and early expansion in the epidermal cell from expression of the HyPer sensor. These time points were rendered in Amira 6.4 utilizing the HyPer fluorescence data to generate a surface that can be overlaid on a green pseudo-colored DIC image of the leaf surface. To image beyond the first epidermal cell layer, it was necessary to move onto a different sample preparation and imaging technique. Tissue clearing permits imaging deeper into the leaf tissue by non-destructively removing chlorophyll and other materials that are within the cells. The technique that was utilized was modified from

ScaleP, which is a urea-based clearing technique.[69] Barley leaves were inoculated as described in previous sections and at specific time points, the leaves were cut such that 1.5 cm sections around the infection site. These leaf sections were put in a 24 well plate with 1 ml fixation solution (2% paraformaldehyde, 2% glutaraldehyde and 0.05% Triton X-100 in 1 X phosphate buffered saline (PBS), pH 7.4), and weighted down with ½ inch polystyrene spheres. The plate was put into a vacuum bell, brought to -30 in HG and left to fix at room temp for 3 hours. The fixation solution and spheres were removed and replaced with 1 X PBS. The vacuum was pulsed off and on until all the samples were fully submerged. Once the all samples stayed at the bottom of the well, the vacuum was pulled, and the bell was moved to 4° C overnight. The following day, the leaves were washed three times with 1X PBS. The tissue clearing began with a treatment of 10% KOH made in 1X PBS. Samples were submerged for 30 minutes, followed by a 3X rinse with 1X PBS, and then an overnight treatment in 0.2 M glycine in 1X PBS to quench autofluorescence caused by the glutaraldehyde. The PBS was then replaced with a stain solution of 0.09 mM Calcofluor White MR2 (CW; Sigma-Aldrich, St. Louis, MO) and 0.026 mM Wheat Germ Agglutinin conjugated to Alexa Fluor 594 (WGA-AF594; Thermofisher Scientific, Carlsbad CA). Previous experiments resulted in unwanted contamination, so to prevent this, 0.005% sodium azide was added. The plates were vacuum bagged and put at 4° C for 5 days. The stain solution was then removed, and the samples were incubated in 2 ml of ScaleP (6 M urea, 30% (v/v) glycerol, and 0.1% (v/v) Triton X-100 in 1 X PBS pH 7.4) for 2 weeks at room temperature. This allowed for optimal clearing of the tissue. Evaporation of the ScaleP solution, the plates were vacuum sealed. Imaging of the samples was done on the Zeiss LSM880, with a Coherent Chameleon Multiphoton Ti:Sapphire laser tuned to 745 nm with a 40X C-

Apochromat (NA 1.2) water immersion objective. The cleared leaf tissue was carefully placed on a droplet of ScaleP, in a 1 well Coverglass bottom Nunc chamber. A glass block was used to keep the leaf section uniformly against the bottom. Emission was split into three channels for the Calcofluor that stains the cell walls (410-490 nm), for the autofluorescence (499- 552 nm) and for the WGA-594 (561-641 nm).

The imaging data was then deconvolved using Hyugens deconvolution software and rendered in Amira 6.4. The hyphal growth, which was only stained with the WGA-594, was isolated out via thresholding and corrected manually using the segmentation editor. This generated a volumetric surface, that would then be displayed clearly over the volume rendering of the leaf data. (Figure 11)

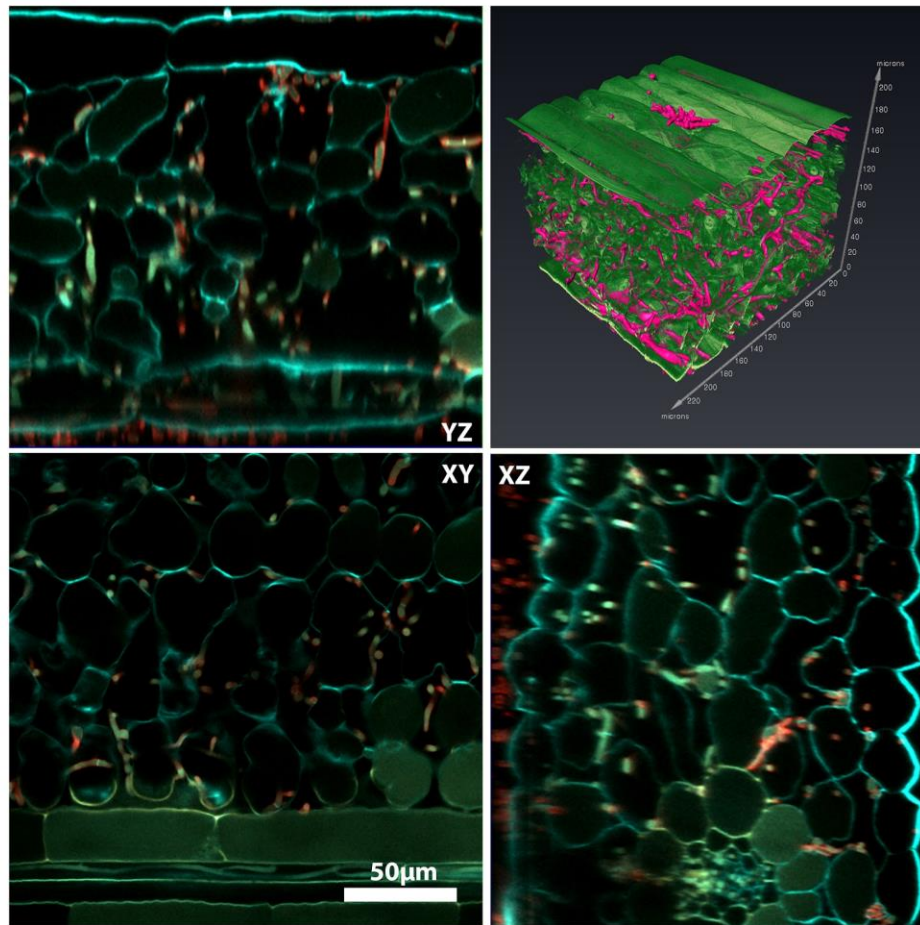


**Figure 11** The volumetric rendering of a *M. oryzae* infection site in barley, 72 HPI. XY, YZ and ZX show single slices from the volumetric dataset. The leaf tissue is shown in cyan; the infection is in red and autofluorescence in the leaf is in yellow. The upper right image shows the fully rendered image in Amira, where the leaf is in green and the hyphae is in pink.

## Chapter 3

### RESULTS

#### 3.1 *M. oryzae* ROS measurement during early stages of the infection cycle

The *M. oryzae* infection cycle has been well described from live and fixed tissue perspectives. [70-72] To understand the levels of ROS during *M. oryzae*'s pathogenesis into barley, live cell data was taken on barley leaves inoculated with the MoHyPer line. These data allowed to track the ROS levels from 2 to 25, as well as 36 and 48 HPI. The ROS ratio from cropped spores and appressoria from the 2-25 HPI datasets were analyzed in Volocity 6.3 and graphed in excel. The quantification of the spores, shown in Figure 12. The same method of quantification was carried out for the appressoria that formed from these spores and is graphed in Figure 13.

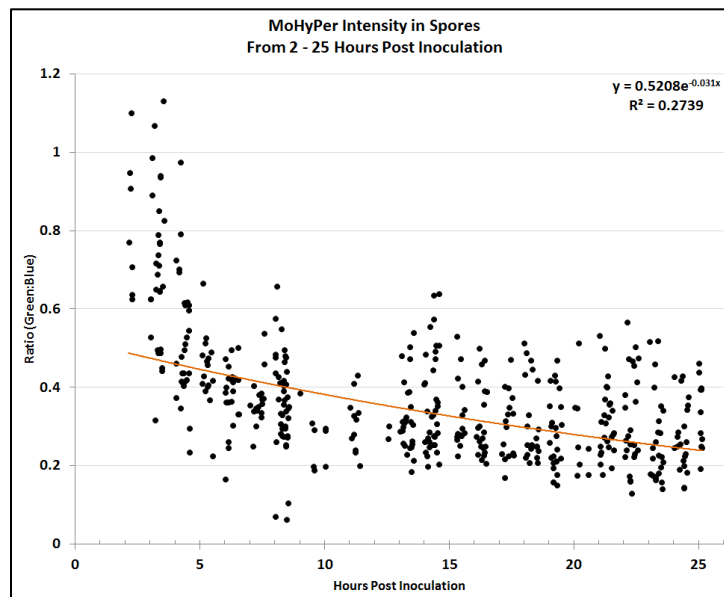


**Figure 12** Quantification of MoHyPer during early stages of pathogenesis in the spores.

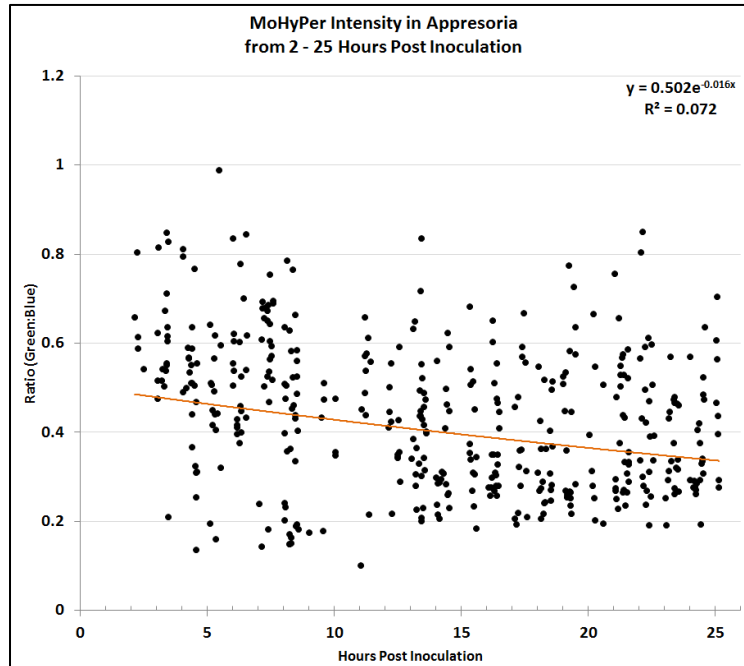


**Figure 13** Quantification of appressorial MoHyPer intensity over early infection stages.

Beyond the early, pre-penetration stages of infection, quantification becomes more challenging as the data becomes more volumetric. Figure 14 shows infection from 36 and 48 HPI time points. Where blue indicates areas of low MoHyPer intensity, and red and white are high levels. Autofluorescence from the plant is also picked up and displayed in the ratio channel. The figure shows a small sampling of the infection sites at both timepoints, and scale bars are 10  $\mu\text{m}$ .

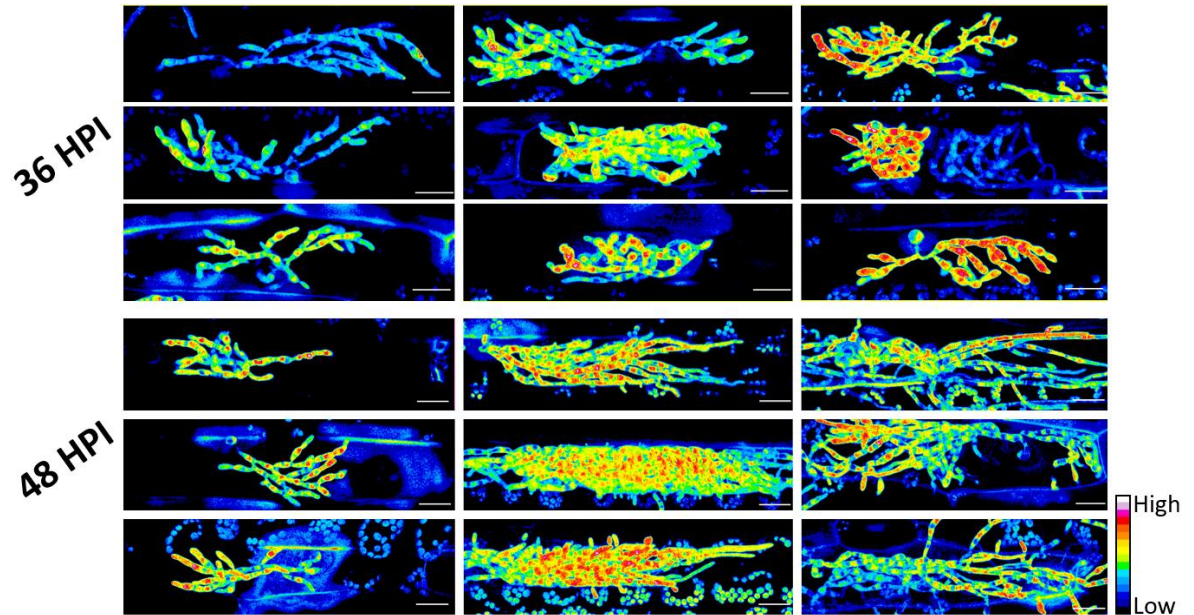


**Figure 14** Selected infection sites, showing a range of MoHyPer intensities at 36 and 48 HPI. The images were generated in FIJI and displayed as the 16 color LUT and scale bars are 10  $\mu\text{m}$ .

### 3.2 Creating a full 3 dimensional infection life cycle for *M. oryzae* on lacey barley

Taking the above quantified ROS data, and paring it with tissue fixation and clearing, allowed for a higher resolution, 3D look at the infection cycle compared to traditional 2 dimensional explanations of *M. oryzae*'s infection cycle. The cleared tissue was imaged on a Zeiss LSM880 multiphoton microscope using a Coherent Chameleon laser tuned to 745 nm. A 3D volume was captured around an infection site, deconvolved using Huygens deconvolution software, and rendered in Amira 6.3.

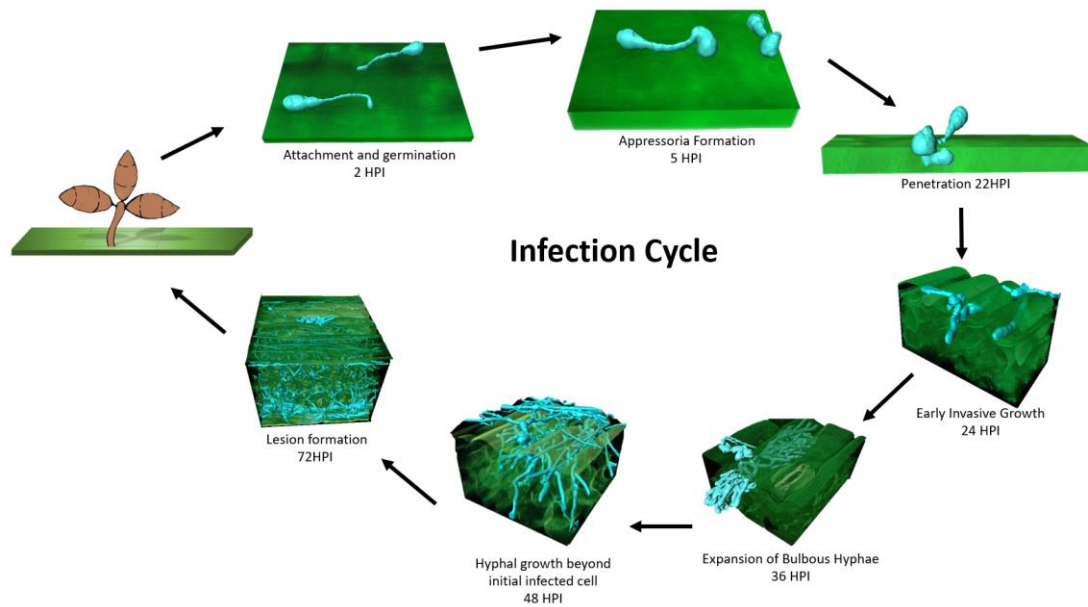


**Figure 15** 3D renderings of only MoHyPer’s infection cycle on lacey barley. Leaf tissue shown in green and fungi shown in cyan. Starting with conidia released from a conidiophore, landing on a leaf’s surface. 2 HPI, germ tubes from the spores are clearly visible. At 5 HPI, early appressoria form, and when 22-24 HPI are reached, *M. oryzae* forms a penetration peg and enters the epidermal cell. At 36 HPI the bulbous hyphae have filled the initial infected cell. 48 and 72 HPI the fungus moves through the leaf tissue and exits. Upon exiting, conidiation will occur and the infection cycle can start over. Inoculated leaf tissue cleared with ScaleP protocol and imaged on Zeiss LSM880 Coherent Chameleon Multiphoton Ti:Sapphire laser tuned to 745 nm with a 40X C-Apochromat (NA 1.2) water immersion lens. Images rendered in Amira 6.3.

### 3.3 *C. heterostrophus*:HyPer inoculation of maize leaves

The *C. heterostrophus*:HyPer is still preliminary, however image data shows that it is possible to successfully capture ROS levels during maize pathogenesis. Figure 16 shows the fluorescence from the HyPer sensor when compared to *C. heterostrophus* wildtype spores 2 HPI on the first leaves of a 20-day old B73 maize plant.

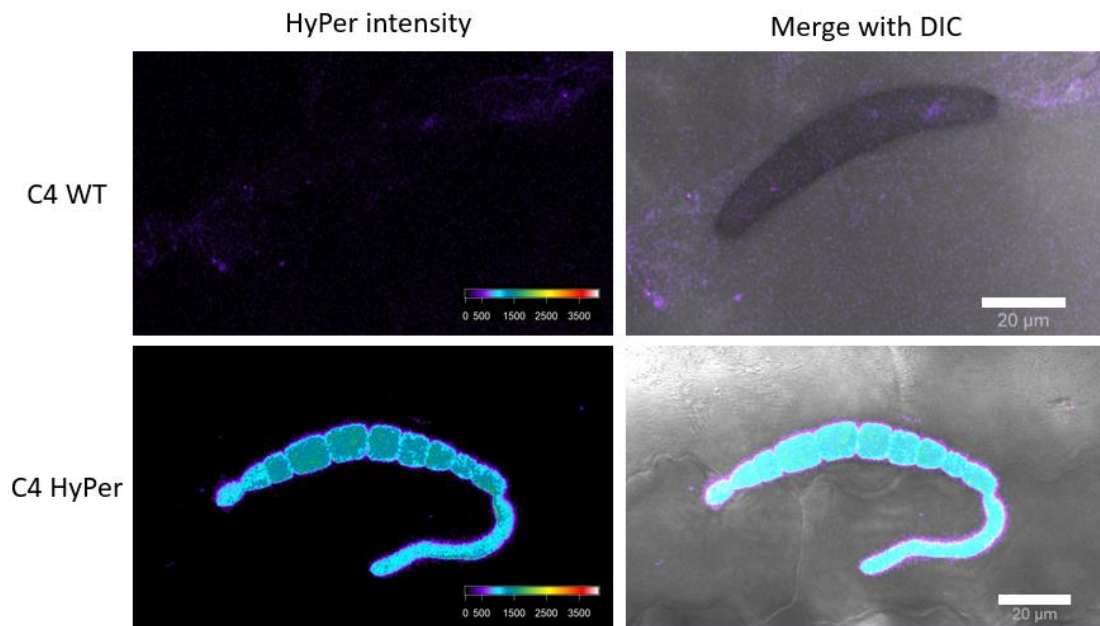


**Figure 16** A comparison of *C. heterostrophus* WT C4 and HyPer expressing lines, 2 HPI on B73 maize first leaves. Upper panels showing lack of fluorescence when compared to the ratiometric output of the HyPer sensor at the same time point.

A comparison was done between B73 (susceptible) and Mo17 (resistant) maize lines to see if there were any noticeable ROS differences. Figure 17 shows one infection site from each maize line 6 hours post inoculation. Images processed in Zen Black.

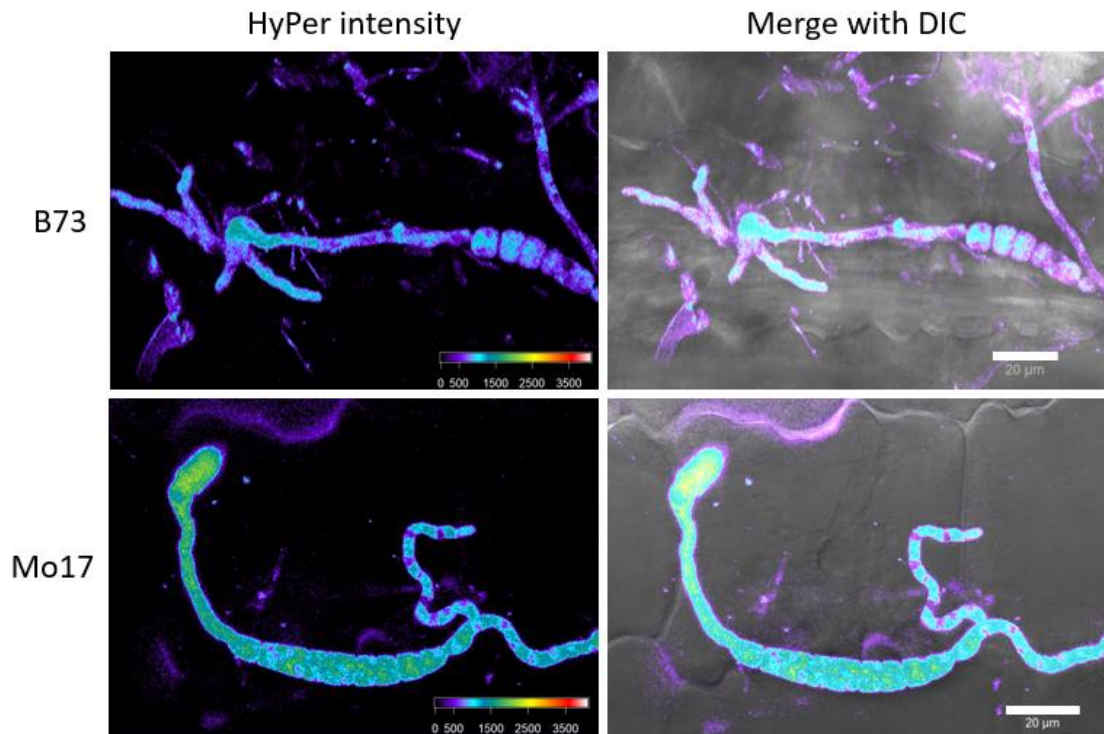


**Figure 17** 6 HPI of *C. heterostrophus*:HyPer on B73 and Mo17 maize lines. Notice that in the upper panel the fungus has made an appressoria and penetrated into B73, while at a similar time on Mo17, there is only an appressoria formed.

### 3.4 Perfusion assays to show ROS response kinetics in *M. oryzae* and *C. heterostrophus*

It is important to understand the response kinetics of wild type MoHyPer expressing *M. oryzae*. Similar research has been performed in *M. oryzae* with roGFP and in *Fusarium graminearum*. [58, 64] Perfusion of multiple solutions over the isolated conidia allowed for real-time measurement in response to these stimuli. One of the initial perfusion experiments conducted was to determine the ideal concentration of H<sub>2</sub>O<sub>2</sub> that would elicit a robust response but not have deleterious effects on the spores. 5, 10, 25, 50 and 100 mM concentrations of H<sub>2</sub>O<sub>2</sub> were flowed across 5 different

coverglasses of isolated conidia. As shown in Figure 18 B-F show the response to this stimulation. 5 mM generates a slightly slower increase in response when compared to 10 mM and higher. Concentrations of 25 mM and higher result in a rapid peak, but the response begins to quickly decrease. Notably in 50 and 100 mM H<sub>2</sub>O<sub>2</sub> there is a slight decrease and then another peak in the response.

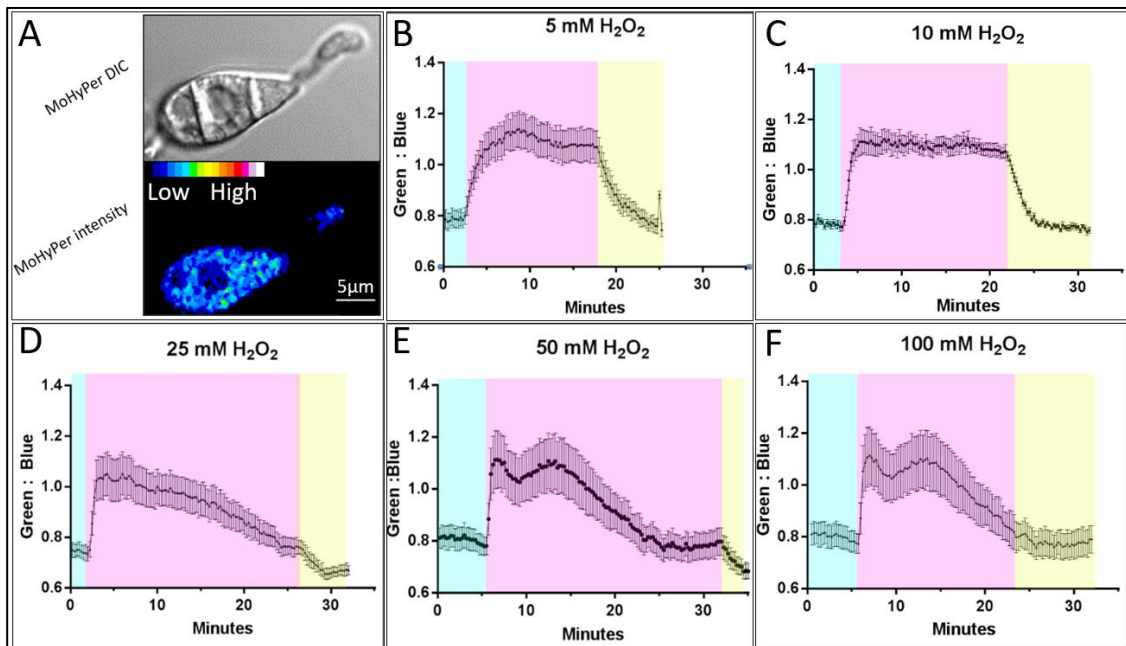


**Figure 18** A. Cropped spore in DIC and ratiometric intensity between 488:405 nm excitation. B-F Differences in response to varied concentrations of H<sub>2</sub>O<sub>2</sub> being flowed through the imaging chamber. Each curve is representative of different spores imaged. Sterile water (blue), 1 mM DTT (yellow) and 10mM H<sub>2</sub>O<sub>2</sub> (pink). Error bars = SD

The 10 mM H<sub>2</sub>O<sub>2</sub> experiment was repeated (Figure 19), in a more controlled manner to allow for uniform analysis between future mutants. 1 mM DTT was added to fully reduce all any free ROS molecules before stimulation. This allows for capturing the full

dynamic range in response to ROS. A similar preliminary analysis (Figure 20) was conducted with the *C. heterostrophus*:HyPer line using only 10 mM H<sub>2</sub>O<sub>2</sub> and 1 mM DTT. The *C. heterostrophus* data represents a curve from a single spore, where each cell of the conidia was treated as a region of interest and quantified in FIJI. To look at the response of multiple conidia to external stimuli, a population of F1 generation from the initial transformation was used to conduct a perfusion experiment. (Figure 22) These conidia were then quantified in Volocity and the response was graphed in GraphPad Prism.

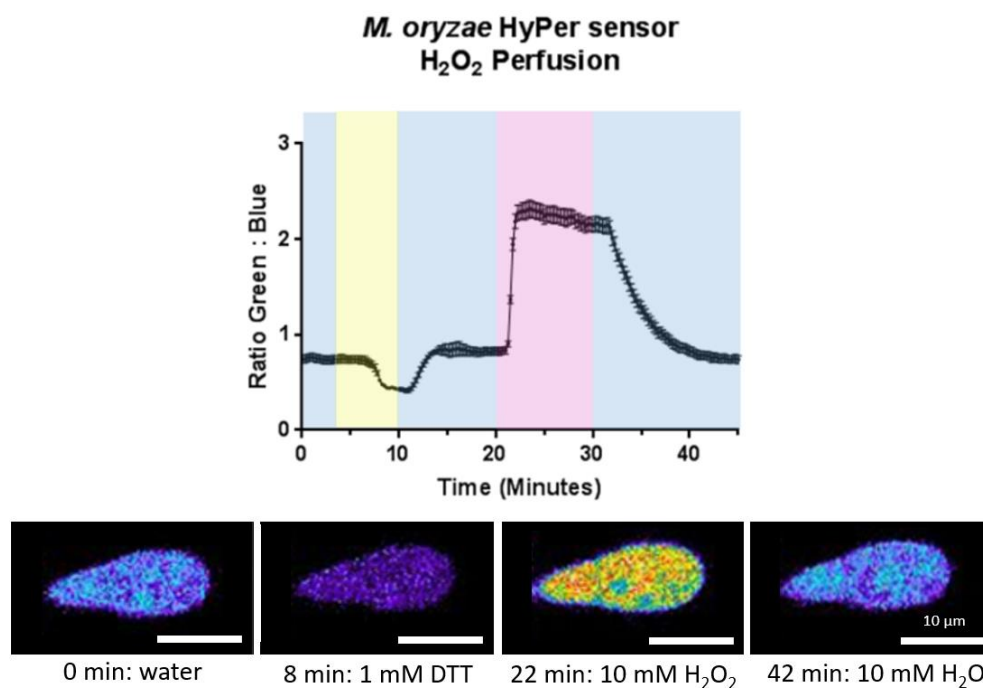


**Figure 19** Perfusion response curve for MoHyPer showing response to sterile water(blue), 1 mM DTT (yellow) and 10 mM H<sub>2</sub>O<sub>2</sub> (pink). Image channel intensity quantified in FIJI and graphed in GraphPad Prism. Spore image processed in Zen. Level of response displayed with rainbow LUT where blue = low and red=high. Scalebar = 10 μm.

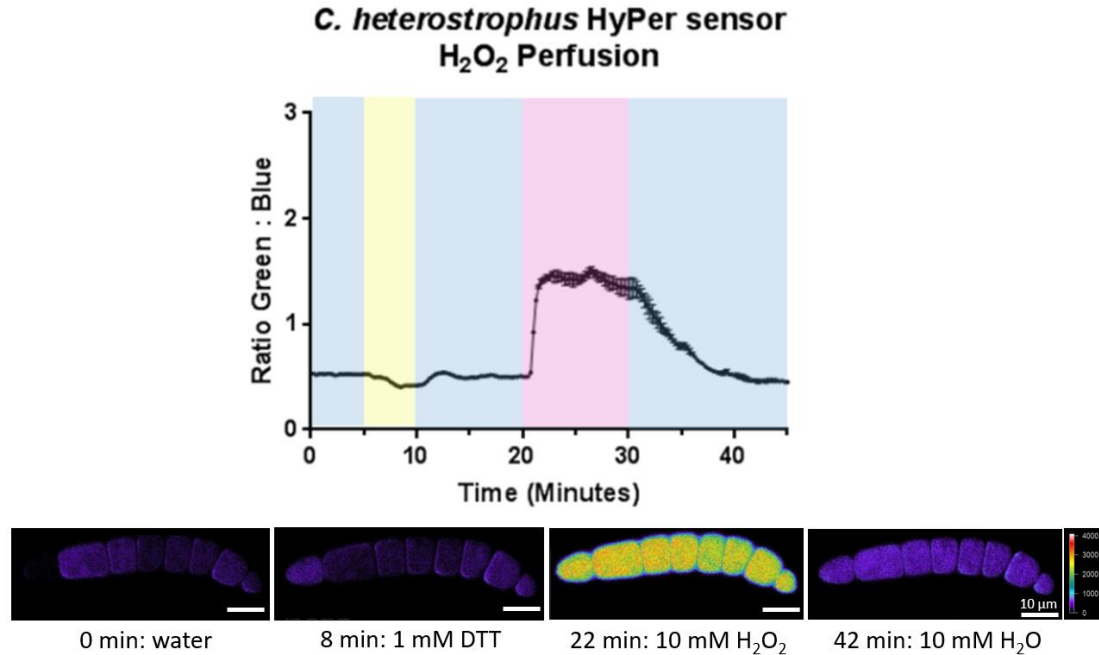


**Figure 20** Perfusion response curve for *C. heterostrophus*:HyPer showing change in HyPer response to sterile water (blue), 1 mM DTT (yellow) and 10 mM H<sub>2</sub>O<sub>2</sub> (pink). Image channel intensity quantified in FIJI and graphed in GraphPad Prism. Spore image processed in Zen. Level of response displayed with rainbow LUT where blue = low and red=high. Scalebar = 10 μm.

During an infection event, the plant does not respond with a single wave of ROS, but rather an initial quick burst followed by a second more sustained burst. [73] To emulate this in the perfusion chamber the same conidia were exposed multiple times to 25 mM of H<sub>2</sub>O<sub>2</sub> to see how the HyPer response changed (Figure 21). The second stimulation results in a similar level of response from the first. However, it trails off more rapidly.

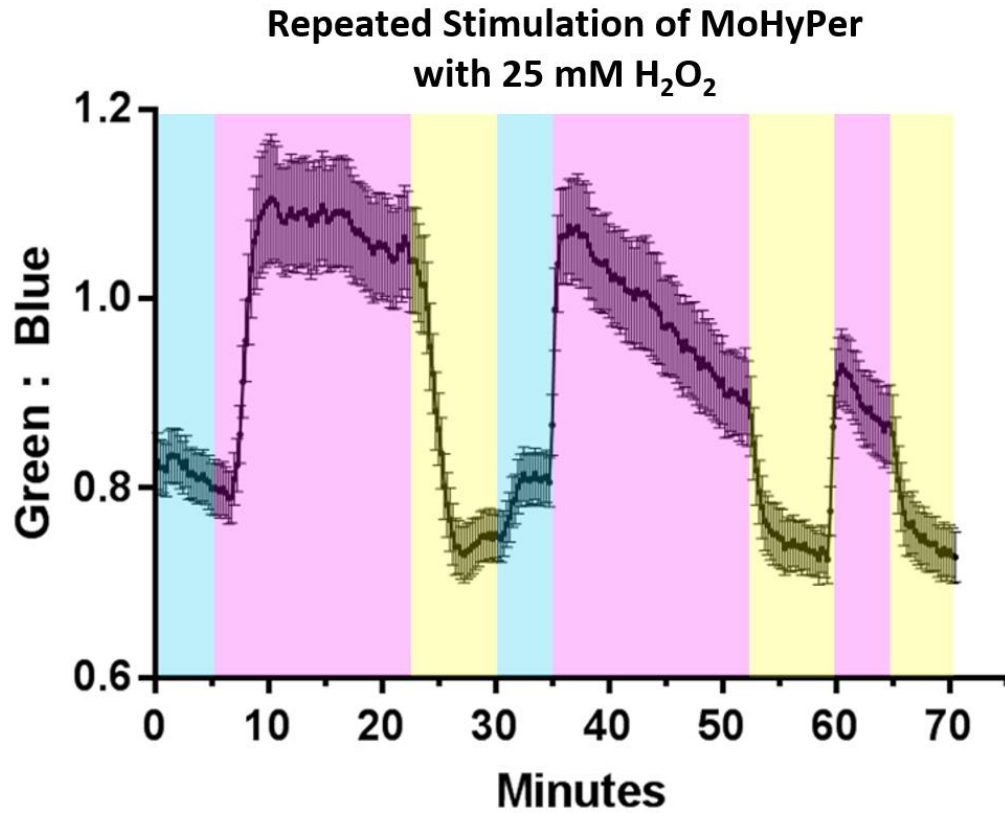


**Figure 21** The same *M. oryzae* conidia were stimulated three times with 25 mM H<sub>2</sub>O<sub>2</sub>. Sustained level of MoHyPer response begins to diminish with the second treatment of H<sub>2</sub>O<sub>2</sub>. Sterile water (blue), 1 mM DTT (yellow) and 10 mM H<sub>2</sub>O<sub>2</sub> (pink).

***C. heterostrophus*:HyPer sensor  
10 mM H<sub>2</sub>O<sub>2</sub> Perfusion**

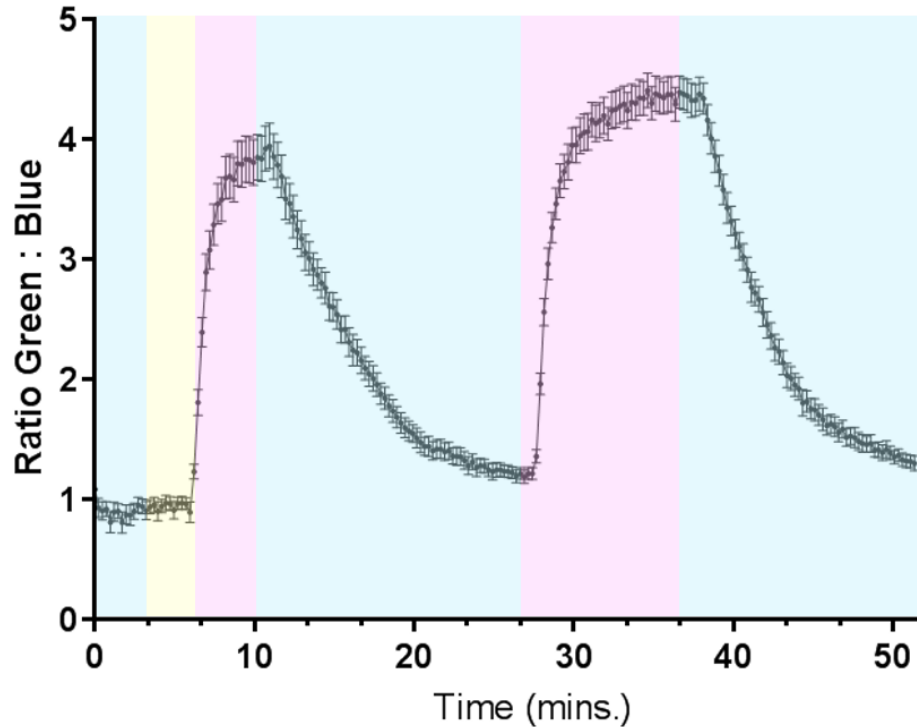


**Figure 22** A mixed population of *C. heterostrophus*:HyPer sensor conidia with two repeated stimulations of 10 mM H<sub>2</sub>O<sub>2</sub>

The primary mutagenesis screen being carried out by Jess Cooper-Pancake and Danielle Mikolajewski is using 140  $\mu$ M menadione to generate ROS during the growth of their random insertion mutants. Menadione generates ROS indirectly by activation by a flavoprotein reductase to a semiquinone. ROS are generated when this semiquinone is oxidized back to a quinone with molecular oxygen. [74] Menadione allows for a consistent production of ROS when compared to adding hydrogen peroxide to the media

because the  $H_2O_2$  will naturally be reduced to form water. A perfusion assay of *M. oryzae* conidia (Figure 22) shows that  $140\ \mu M$  menadione dissolved in 95% EtOH does indeed stimulate the spores and generate ROS. Menadione powder is not soluble in water, so the water-soluble form, menadione sodium bisulfite (MBS) was used in a perfusion assay. (Figure 23) For conformation of functioning MoHyPer in this assay,  $10\ mM\ H_2O_2$  was added at the end.

### MoHyPer response to $140\ \mu M$ Menadione in 95% EtOH

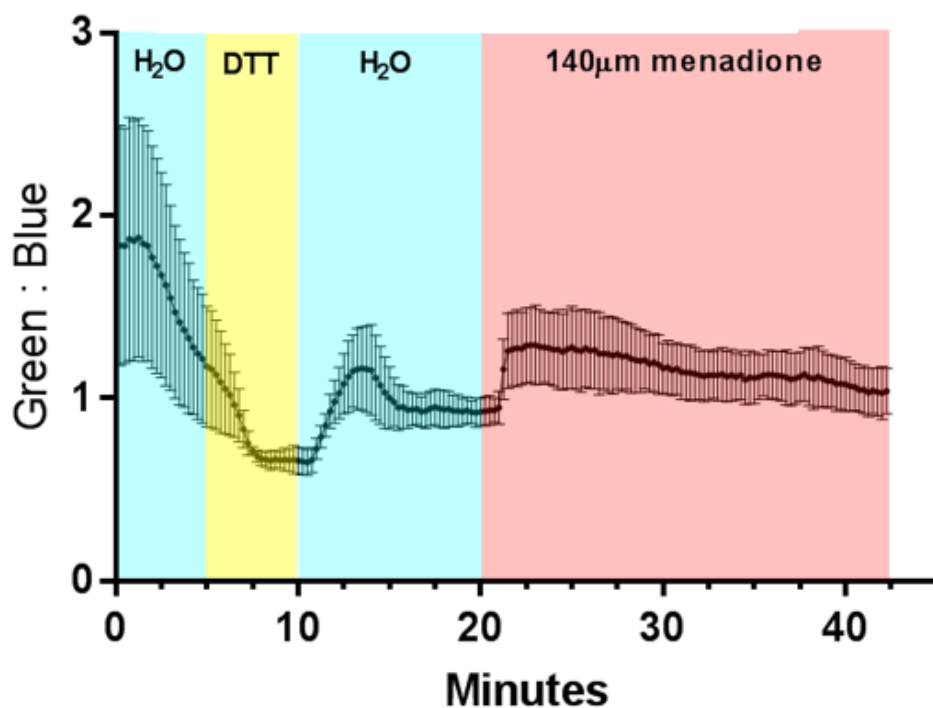


**Figure 23** Perfusion assay of MoHyPer with  $140\ \mu M$  menadione. Sterile water(blue),  $1\ mM$  DTT (yellow) and  $140\ \mu M$  Menadione in 95% EtOH (red).

The MoHyPer response to the MBS was very minimal at 140  $\mu\text{M}$  and 1 mM. There was a slight increase seen at 10 mM, but it was not as robust as adding 10 mM  $\text{H}_2\text{O}_2$ , which was done at the end of the experiment to show that the spores were viable, and the HyPer sensor was functioning properly.

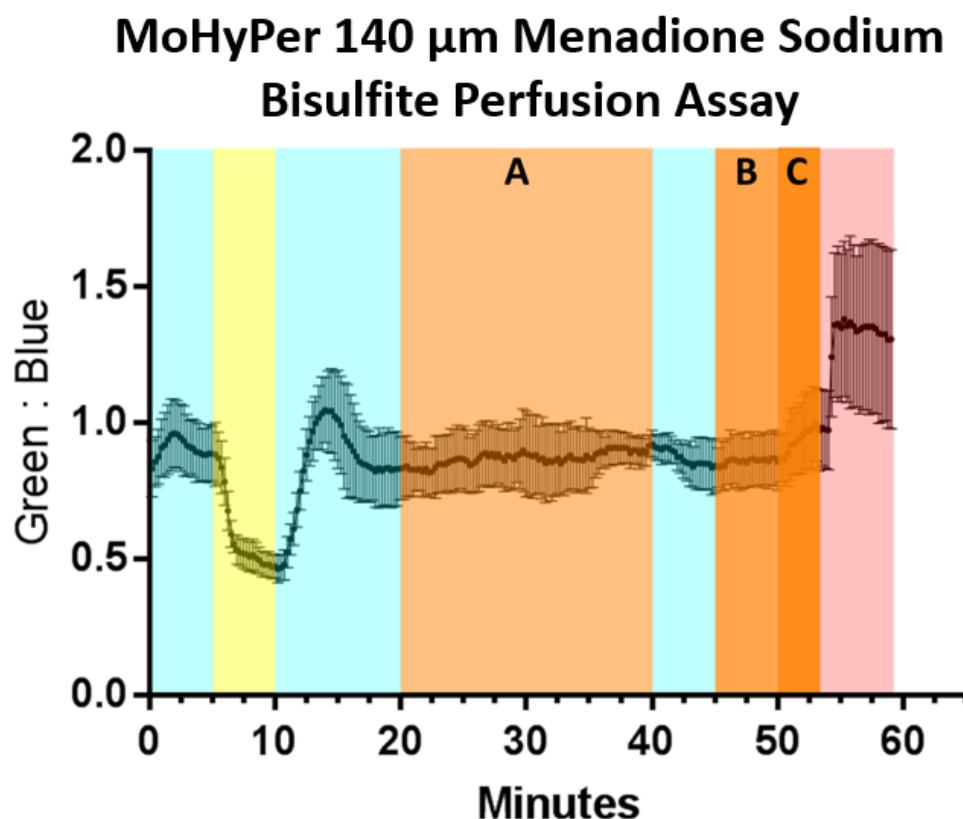


**Figure 24** Perfusion assay of menadione sodium bisulfite (MBS). A - C 140  $\mu\text{M}$ , 1 mM and 10 mM MBS respectively. Sterile water(blue), 1 mM DTT (yellow) and 10 mM  $\text{H}_2\text{O}_2$  (pink).

In the original Belousov *et al* article, it was shown that the HyPer sensor was sensitive to pH levels above 8. To see if this was the case in both of these transgenic

fungal species, a perfusion assay was conducted with 1XPBS of differing pH concentrations. Figure 25 and 26 show the response curves of both pathogens.

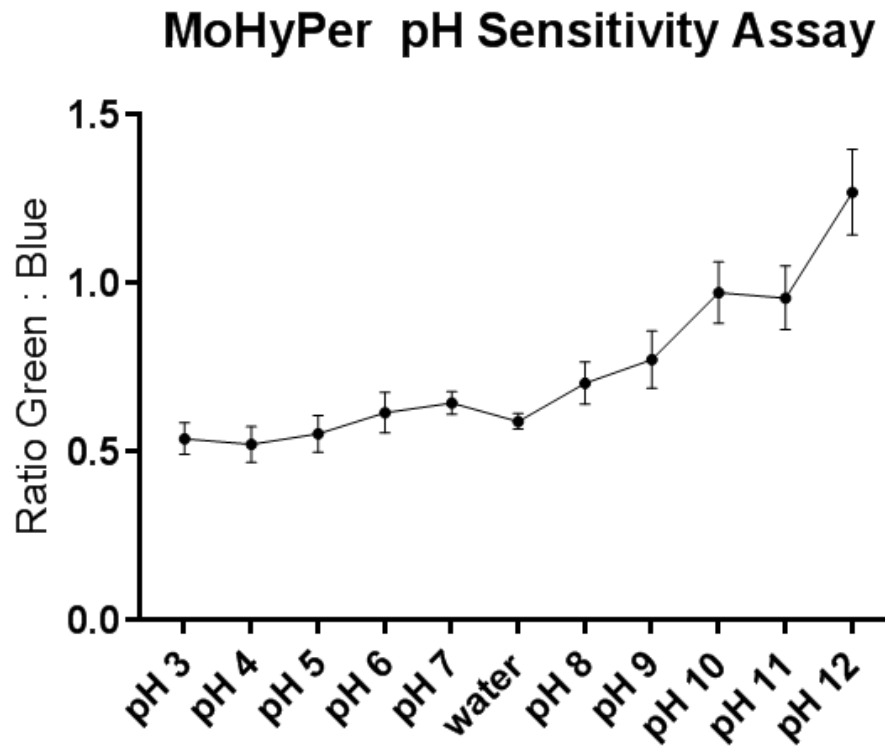


**Figure 25** Perfusion assay showing the sensitivity of MoHyPer in response to pH extremes. Response is significant. p-value <0.001

### *C. heterostrophus* HyPer sensor pH sensitivity assay

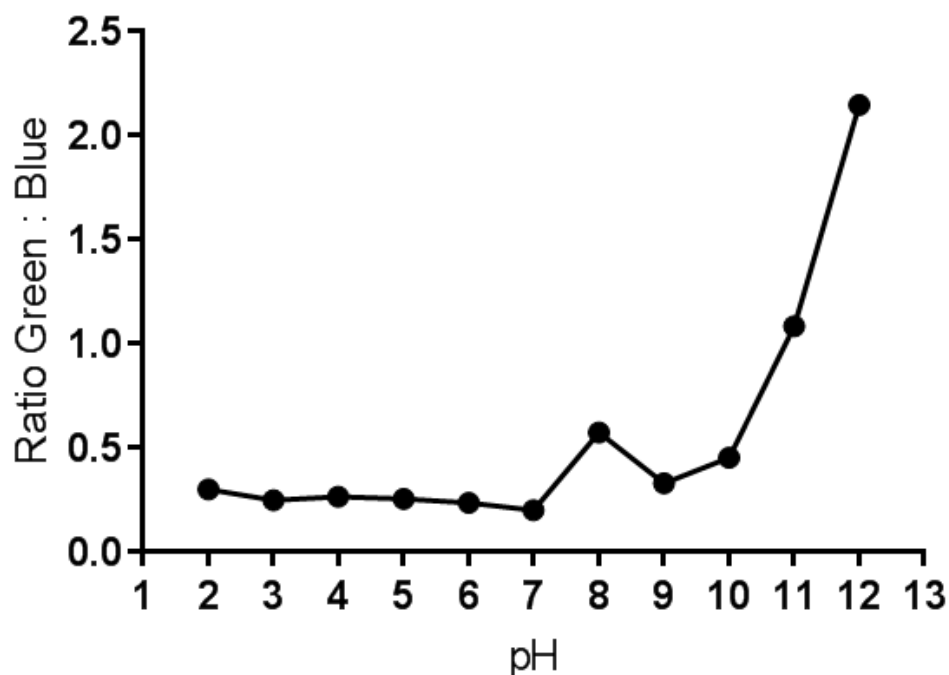


**Figure 26** *C. heterostrophus*:HyPer single conidia treated with 1 X PBS buffers of different pH concentrations.

#### 3.5 High throughput assay development for *M. oryzae* mutant screening

For analysis of random insertion mutants being generated in the lab, there was a need for the development of a high throughput assay. Using the ThermoFisher CX7 high content imager allows for rapid screening and automatic segmentation of objects. A protocol was developed in the software to segment the spores based off size and shape, measuring the average intensity at 405 nm and 488 nm excitations. An initial assay was performed with 0, 5, 10, 25 and 50 mM H<sub>2</sub>O<sub>2</sub> in quadruplicate. There were two goals for this experiment. The first was to confirm the concentration measurements from the

confocal experiments, were consistent on a wide-field imaging system. The second was to see how time impacted the consistency in the ROS response. The response of these three assays was quantified within the CX7 software, and the graphed in Excel.

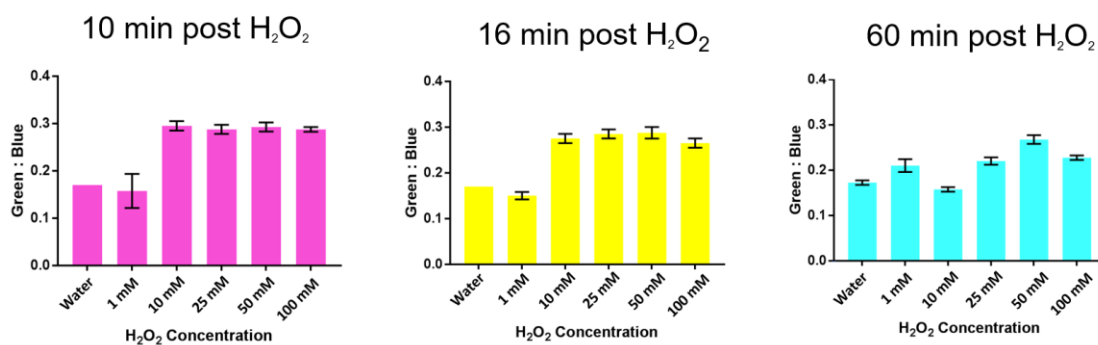


**Figure 27** *M. oryzae* spores plated in quadruplicate were imaged three times over an hour to measure the consistency of HyPer response over an extended period. Error bars = SD

## Chapter 4

### DISCUSSION

#### 4.1 Analysis of fungal HyPer sensor kinetics in an *in vitro* environment

*M. oryzae* and *C. heterostrophus* are two model systems to elucidate the potential differences in hemi-biotrophic and necrotrophic fungal lifestyles. The ability of stable expression of the HyPer sensor within these organisms permits a real-time view into ROS level dynamics when exposed to exogenous stimuli and during host interactions.

The host interaction for *M. oryzae* was begun at 2 HPI to ensure that enough spores had time to attach to the leaf surface. Figure 12 displays the MoHyPer ratio of cropped spores through germination time shows a decrease in ROS levels. The germ tube extension away from the conidia stops after roughly 4 hours, start “hooking” and forming an appressoria. [12, 75] The negative exponential curve makes sense when thinking about ROS as a bioproduct for energetic production. Once the germ tube extension is complete and appressorial formation occurs, it was expected to see an increase in ROS within the appressoria. It has been previously published that the NOX genes play an important role in appressorial formation and generation of the penetration peg.[9] However, when graphed in Figure 13, there does not appear to be a clear trend in the data. This could be that the ROS burst is too rapid or faint to be captured on our Zeiss LSM710 confocal. Another possibility is the ROS levels do not peak until the invasive hyphae being a complete invasion of the first epidermal cell. The time points that were collected for these images end right when penetration of the first cell is occurring, so perhaps later timepoints would allow any increase to be visualized.

Moving on beyond the early infection stages, to where *M. oryzae* has entered the host and is moving beyond the first epidermal cell, Figure 14 shows a snapshot of infection sites at 36 and 48 HPI. From these images it is clear to see a wide range in MoHyPer levels. The timepoints are rough approximations of when these infection sites started since it is impossible to precisely know when a conidia lands, germinates and enters the host. The 36 HPI data is showing invasive hyphae that are still cloaked in the host plasma membrane. [10] At 48 HPI the host PM is lost and the hyphae are moving cell to cell, where they be experiencing more potential host ROS. Since we do not have an analogous sensor within the leaf tissue, it is not possible to determine if the levels of increased ROS are responsive to the environment or generated within the fungi. It could be beneficial to add a stain for the host cytoplasm (FM-464) to see if there is an increase in ROS detection related to the hyphae being coated in host membrane. By pairing the early infection data with advanced clearing techniques, it was possible to generate a 3D infection cycle for *M. oryzae*. While the data did not elucidate anything novel about *M. oryzae* pathogenesis on barley, it is the first of such diagram generated for any plant pathogen.

#### **4.2 *In vitro* ROS kinetics for MoHyPer and *C. heterostrophus*:HyPer**

For a comparison of the ROS levels and kinetics in both of these fungi, it was necessary to make a stable transformation of *C. heterostrophus* to carry the HyPer sensor. This had been previously accomplished by the Horwitz lab in 2013.[53] Since the Horwitz lab is in Israel, it was going to be extremely challenging and time consuming to get a permit to import this strain into The United States. However, I was able to receive the same version of the HyPer sensor plasmid that was transformed in the Ronen *et al* paper. With assistance from Jon González in the Turgeon lab at Cornell,

we were able to successfully transform C4 *C. heterostrophus*. Multiple transformants were generated and glycerol stocked for future use. The first experiment for these new lines was to determine the functionality of *C. heterostrophus*:HyPer. This is shown in Figure 16, where the upper panel is a WT conidia and the lower panel is *C. heterostrophus*:HyPer on a B73 leaf 2 HPI. The expression is clearly visible in the transgenic line. Utilizing the *C. heterostrophus*:HyPer line, 20 day old B73 and Mo17 plants were inoculated and imaged. Figure 17 shows a comparison of one infection each site from these plants. Previous published data showed that Mo17 is more resistant to this race of *C. heterostrophus*. [76] It can be seen that the infection site on the B73 plant in Figure 17 entered the host tissue while the conidia on Mo17 has only formed an appressoria. The intensity of the HyPer sensor is increased in the Mo17 infecting conidia, however much more data will need to be acquired to conclude if this is a real trend.

### **4.3 *In vitro* analysis of ROS kinetics using open perfusion system.**

For understanding of the HyPer sensor kinetics independent of plant signaling and defense, an *in vitro* approach was taken. This ensured that only the response to H<sub>2</sub>O<sub>2</sub> was being observed. The first experiment that was performed was assaying different H<sub>2</sub>O<sub>2</sub> concentrations through the perfusion system. Five separate conidial isolations were exposed to five different H<sub>2</sub>O<sub>2</sub> concentrations (5, 10, 25, 50 and 100 mM). From these data in Figure 18, it is possible to see that MoHyPer can tolerate 5 and 10 mM, but >25 mM results in a peak and then a steady drop off. The trend in the drop off of these peaks are similar to the Samalova *et al* paper looking at Ro-GFP in *M. oryzae*. [58] Ro-GFP is measuring the redox state of the cell by reacting with the intracellular glutathione pools. In *Fusarium graminearum*, HyPer-2, a form of the HyPer sensor with

an expanded dynamic range, was used in and when treated with 50 mM H<sub>2</sub>O<sub>2</sub>, the response curve had a comparable peak and drop off. [64, 66] A possible reason for this is saturation of the sensors, beyond what is biologically experienced in a fungal:host interaction which can be on the nmol to μmol range [77]. It was determined that 10 μM generated a nice curve for future mutant analysis, so this was repeated generating the MoHyPer kinetic plot that is seen in Figure 19. The same 10 μM H<sub>2</sub>O<sub>2</sub> treatment was used on *C. heterostrophus*:HyPer and a similar plot was created, Figure 20. While this plot does not have the same level of increase when compared to MoHyPer in Figure 19, an experiment showing repeated stimuli of *C. heterostrophus*:HyPer (figure 22) has a greater increase than what is seen in MoHyPer normally. It is unclear what is the cause of this difference.

To further push MoHyPer's H<sub>2</sub>O<sub>2</sub> tolerance, conidia were repeatedly treated with 25 mM H<sub>2</sub>O<sub>2</sub> in the perfusion system to see the effects on a strong stimulation. This resulted in peaks that were successively decreased as seen in Figure 21. The likely reason for this is MoHyPer did not have time to recover from this intense stimulus, so the following treatments were exhausting the conidia's detoxification ability. Again, these curves have a similar shape to the RoGFP curves in Samalova *et al.* However, their data shows increasing RoGFP levels successive treatments with increasing H<sub>2</sub>O<sub>2</sub>, indicating they have not saturated their sensors detection range.

ROS stimulation for cells is possible in multiple means, a common chemical used is menadione. This indirect generation of H<sub>2</sub>O<sub>2</sub> can be more stable since it will not be reduced to water and is a good choice for long term experiments. To see the effect of menadione on MoHyPer, 140 μM was perfused across spores resulting in a slight activation of the sensor. The graph of this data in Figure 23, starts with a high peak in

the H<sub>2</sub>O wash, which is likely due to residual H<sub>2</sub>O<sub>2</sub> being in the line from previous experiments. A concern for this experiment was menadione's solubility. The stock solution is prepared in 95% ethanol, and when it is added to water, a small amount precipitates out, making it difficult to know the actual final concentration. Menadione sodium bisulfite was tried in a perfusion assay, Figure 24, but at 140 μM it did not result in stimulation of the sensor. The concentration was increased to 1 mM and 10 mM with little change in the MoHyPer intensity. A final addition of 10 mM H<sub>2</sub>O<sub>2</sub> was flushed into the system to confirm that the sensor was still active.

It was shown in the original paper that the HyPer sensor had sensitivity to pH extremes. Since pH does play a role in a host: pathogen interaction, and has been shown to change during *M. oryzae* germination, it was necessary to evaluate our HyPer sensor lines for pH sensitivity. [78, 79] 1 X PBS of varying pH was flowed across conidia and quantified. MoHyPer in Figure 25 and *C. heterostrophus*:HyPer in figure 26 both show an increase in the sensor activity when the pH increases above 8. This sensitivity in the HyPer sensor has been addressed by the creation of SypHer which is used as a pH control. SypHer is H<sub>2</sub>O<sub>2</sub> insensitive, so when used as a control, any change in fluorescence is in response to pH and not ROS detection

The final in vitro analysis that was performed with MoHyPer was the generation of a high throughput assay that can be used for future mutant screen analysis. The ThermoFisher CX7 high content imager makes it possible to image 96 well, coverglass bottom plates in an automated manner. It is possible to run the system in a widefield or a confocal mode. The widefield mode was selected to capture the whole volume of the spore easily. During the initial setup of the assay, the assay was optimized for the 20X 0.7NA air objective. At this magnification it is possible to detect spores, and see the

intensity of the HyPer sensor, however the resolution does not show much detail about the cellular contents. Preliminary images were taken, where the intensity, size and shape of the conidia were used to determine the parameters that the software will use to identify and count spores during imaging. After it was clear that the system could visualize and count the spores, the next step was performing a titration of H<sub>2</sub>O<sub>2</sub> concentrations. Spores were isolated and allowed to adhere to the 96-well plate for 30 minutes in the dark. After which, the H<sub>2</sub>O<sub>2</sub> was added to wells in quadruplicate. The plate was put into the CX7 and the assay was begun. A minimum of 300 spores or a total of 18 fields were imaged, whichever came first. The run took a little less than 16 minutes before the next run was initiated. This was to see the reproducibility of the assay conditions. A final run was done 60 minutes post addition of H<sub>2</sub>O<sub>2</sub>. What is shown in Figure 27 is a consistency between the first two runs at all concentrations, but after an hour the MoHyPer signal becomes unreliable and noisy. This served to eliminate the potential use of the CX7 plate stacker, which would have allowed us to load up dozens of plates and let the system run through them automatically.

#### 4.4 Conclusions

*M. oryzae* and *C. heterostrophus* have much to teach us about fungal redox biology. With the addition of the HyPer sensor as a tool for visualizing this important transient molecule, it will be possible to further understand the role ROS plays during pathogenesis. The *in planta* assay showed a negative trend in ROS levels during spore germination, but lacked a clear correlation during appressorial formation. It is possible that analyzing that data in another manner will make it possible to quantify any change in MoHyPer levels. A similar analysis during pathogenesis will need to be performed on maize with the *C. heterostrophus*:HyPer. This should be performed on both B73 and

Mo17 since these maize lines have been genetically characterized thoroughly, and this information may help future line breeding.

The kinetic analysis has created a benchmark which can be used to assay mutants and specific gene knockouts in *M. oryzae*. More perfusion assays will need to be performed to see the effects of lesser H<sub>2</sub>O<sub>2</sub> levels for longer times or repeated stimulations. Is there really a peak that then rapidly decreases or is the sensor getting overwhelmed? Other imaging techniques will need to be investigated for imaging MyHyPer levels during appressorial formation. It is possible that using super resolution microscopy, it may be possible to capture ROS bursts or intracellular gradients. Further kinetic analysis will need to be carried out with in *C. heterostrophus*, such as tolerance assays for minimum and maximum H<sub>2</sub>O<sub>2</sub> concentrations that can be detected, effects of repeated stimulation and kinetics of different ROS generating chemicals like menadione. It is also necessary to transform SypHer into both fungal systems, there is a proper pH control for all assays. With these data, it will be possible to determine the fungal ROS kinetics of both pathogens during host interactions. From here analysis with resistant and susceptible hosts can allow for the development of more robust crop lines.

## REFERENCES

If you want to number your bibliographic entries, change the style of the items to *Bib Entry - numbered*.

1. FAOSTAT (Food and Agriculture Organization of the United Nations, 2018.
2. Savary, S., et al., *The global burden of pathogens and pests on major food crops*. Nat Ecol Evol, 2019. **3**(3): p. 430-439.
3. Bruinsma, J., *What are the likely developments in world agriculture towards 2050?* Global Forum on Agricultural Research (GFAR), 2012(38).
4. Yoshida, K., et al., *Host specialization of the blast fungus Magnaporthe oryzae is associated with dynamic gain and loss of genes linked to transposable elements*. BMC Genomics, 2016. **17**: p. 370.
5. Wilson, R.A. and N.J. Talbot, *Under pressure: investigating the biology of plant infection by Magnaporthe oryzae*. Nat Rev Microbiol, 2009. **7**(3): p. 185-95.
6. Yoshinobu Ebata, H.Y., Takeo Uchiyama *Chemical Composition of the glue from appressoria of Magnaporthe oryzae*. Bioscience, biotechnology and biochemistry 1998. **Vol 62**: p. 672-674.
7. Perez-Nadales, E., et al., *Fungal model systems and the elucidation of pathogenicity determinants*. Fungal Genet Biol, 2014. **70**: p. 42-67.
8. Jong, J.C.d., et al., *Glycerol generates turgor in rice blast*. Nature. **389**.
9. Ryder, L.S., et al., *NADPH oxidases regulate septin-mediated cytoskeletal remodeling during plant infection by the rice blast fungus*. Proc Natl Acad Sci U S A, 2013. **110**(8): p. 3179-84.
10. Khang, C.H., et al., *Translocation of Magnaporthe oryzae effectors into rice cells and their subsequent cell-to-cell movement*. Plant Cell, 2010. **22**(4): p. 1388-403.
11. Zhang, S. and J.R. Xu, *Effectors and effector delivery in Magnaporthe oryzae*. PLoS Pathog, 2014. **10**(1): p. e1003826.
12. Oses-Ruiz, M., et al., *Two independent S-phase checkpoints regulate appressorium-mediated plant infection by the rice blast fungus Magnaporthe oryzae*. Proc Natl Acad Sci U S A, 2017. **114**(2): p. E237-E244.
13. Kubicek, B.A.H.P.K.M.M.C.P., *Genomics of Soil- and Plant-Associated Fungi*. Soil Biology, 2013. **Vol 36**: p. 213-228.
14. Drechsler, C., *Leafspot on maize caused by Ophiolobus heterostrophis, N. SP., the ascigerous stage of Helminthosporium exhibiting bipolar germination*. . Journal of Agricultural Research, 1925. **XXXI**: p. 701-725.
15. Wise, R.P., et al., *The Genetics, Pathology, and Molecular Biology of T-Cytoplasm Male Sterility in Maize*, in *Advances in Agronomy Volume 65*. 1999. p. 79-130.
16. OLEN C. YODER, K.K., *Molecular Genetics Of Host-Specific Toxins*.

17. HOOKER, S.M.L.A.A.L., *Southern Corn Leaf Blight: Genetic Control of Pathogenicity and Toxin Production in Race T and Race O of Cochliobolus heterostrophus*. Genetics. **69**: p. 115-117
18. Gao Zhihuan, X.Y., Dai Jingrui, *The pathogenic site of the C-toxin derived from Bipolaris maydis race C in maize (Zea mays)*. Chinese Science Bulletin. **Vol. 45**( No. 19): p. 1787- 1791.
19. K. Mendgen, M.H., and H. Deising, *Morphogenesis and mechanisms of penetration by plant pathogenic fungi*. Phytopathology, 1996. **34**: p. 367–86.
20. Yoder, O.C., *Cochliobolus heterostrophus, cause of southern corn leaf blight*. . Advances in Plant Pathology, 1988. **6**: p. 93-112.
21. Zipfel, C., *Pattern-recognition receptors in plant innate immunity*. Curr Opin Immunol, 2008. **20**(1): p. 10-6.
22. Macho, A.P. and C. Zipfel, *Plant PRRs and the activation of innate immune signaling*. Mol Cell, 2014. **54**(2): p. 263-72.
23. Dorey, S.e.a., J.D. Jones, and J.L. Dangl, *The Plant Immune system*. Nature, 2006. **444**(7117): p. 323-9.
24. Han, G.Z., *Origin and evolution of the plant immune system*. New Phytol, 2019. **222**(1): p. 70-83.
25. Conrath, U., *Systemic Acquired Resistance*. Plant Signaling & Behavior, 2006. **1**: p. 179-184.
26. Cao, H., et al., *The Arabidopsis NPR1 Gene That Controls Systemic Acquired Resistance Encodes a Novel Protein Containing Ankyrin Repeats*. Cell, 1997. **88**(1): p. 57-63.
27. Heller, J. and P. Tudzynski, *Reactive oxygen species in phytopathogenic fungi: signaling, development, and disease*. Annu Rev Phytopathol, 2011. **49**: p. 369-90.
28. Abdul Wahid, M.F., and Kadambot H.M. Siddique, *Implications of oxidative stress for plant growth and productivity*. Handbook of Plant and Crop Physiology. **Third Edition**: p. 549-556.
29. Huang, K., *A Study of Genes Involved in Redox Regulaion During Magnaporthe-Host Interaction* ProQuest LLC 2012.
30. Treml, J. and K. Šmejkal, *Flavonoids as Potent Scavengers of Hydroxyl Radicals*. Comprehensive Reviews in Food Science and Food Safety, 2016. **15**(4): p. 720-738.
31. Abdul Wahid, M.F., and Kadambot H.M. Siddique, *Implications of Oxidative Stress for Crop Growth and Productivity*. Handbook of Plant and Crop Physiology.
32. Bruce ALberts, A.J., Julian Lewis, Martin Raff, Keith Roberts, Peter Walters, *Molecular Biology of the Cell, Fifth Edition*. 2008: p. 868.
33. Patricia Muñler, X.-P.L., and Krishna K. Niyogi\*, *Non-Photochemical Quenching. A Response to Excess Light Energy*. Plant Physiology, 2001. **125**: p. 1558-1566.

34. Triantaphylides, C., et al., *Singlet oxygen is the major reactive oxygen species involved in photooxidative damage to plants*. *Plant Physiol*, 2008. **148**(2): p. 960-8.
35. Achim Trebsta, B.D., Heike Hollander-Czytko, *A specific role for tocopherol and of chemical singlet oxygen quenchers in the maintenance of photosystem II structure and function in Chlamydomonas reinhardtii*. Federation of European Biochemical Societies. **516** p. 156-160.
36. Liochev, S.I. and I. Fridovich, *The Haber-Weiss cycle -- 70 years later: an alternative view*. *Redox Rep*, 2002. **7**(1): p. 55-7; author reply 59-60.
37. Das, K.C. and C.K. Das, *Thioredoxin, a Singlet Oxygen Quencher and Hydroxyl Radical Scavenger: Redox Independent Functions*. *Biochemical and Biophysical Research Communications*, 2000. **277**(2): p. 443-447.
38. Apel, K. and H. Hirt, *Reactive oxygen species: metabolism, oxidative stress, and signal transduction*. *Annu Rev Plant Biol*, 2004. **55**: p. 373-99.
39. Noctor, G., J.P. Reichheld, and C.H. Foyer, *ROS-related redox regulation and signaling in plants*. *Semin Cell Dev Biol*, 2018. **80**: p. 3-12.
40. Torres, M.A., J.D. Jones, and J.L. Dangl, *Reactive oxygen species signaling in response to pathogens*. *Plant Physiol*, 2006. **141**(2): p. 373-8.
41. WOJTASZEK, P., *Oxidative burst : an early plant response to pathogen infection*. *Biochemistry*, 1997. **332**: p. 681–692.
42. Zamocky, M., P.G. Furtmüller, and C. Obinger, *Evolution of Catalases from Bacteria to Humans*. *Antioxidants & Redox Signaling*, 2008. **Vol 10**(No. 9): p. 1527-1547.
43. Sies, H., *Hydrogen peroxide as a central redox signaling molecule in physiological oxidative stress: Oxidative eustress*. *Redox Biol*, 2017. **11**: p. 613-619.
44. Bailey-Serres, J. and R. Mittler, *The roles of reactive oxygen species in plant cells*. *Plant Physiol*, 2006. **141**(2): p. 311.
45. Able, A.J., *Role of reactive oxygen species in the response of barley to necrotrophic pathogens*. *Protoplasma*, 2003. **221**(1-2): p. 137-43.
46. Mhamdi, A., G. Noctor, and A. Baker, *Plant catalases: peroxisomal redox guardians*. *Arch Biochem Biophys*, 2012. **525**(2): p. 181-94.
47. Lev, S., et al., *Activation of an API-like transcription factor of the maize pathogen Cochliobolus heterostrophus in response to oxidative stress and plant signals*. *Eukaryot Cell*, 2005. **4**(2): p. 443-54.
48. SEAN T. COLEMAN, E.A.E., SUSANNE M. STEGGERDA, AND W. SCOTT MOYE-ROWLEY, *Yap1p Activates Gene Transcription in an Oxidant-Specific Fashion*. *Molecular and Cellular Biology*. **Vol 19**: p. p. 8302–8313.
49. Kuge, S., et al., *Regulation of the Yeast Yap1p Nuclear Export Signal Is Mediated by Redox Signal-Induced Reversible Disulfide Bond Formation*. *Molecular and Cellular Biology*, 2001. **21**(18): p. 6139-6150.

50. Shusuke Kuge, N.J.a.A.N., *Regulation of yAP-1 nuclear localization in response to oxidative stress*. The EMBO Journal 1997. **Vol.16**: p. pp.1710–1720.
51. Rodrigues-Pousada, C., R.A. Menezes, and C. Pimentel, *The Yap family and its role in stress response*. Yeast, 2010. **27**(5): p. 245-58.
52. Guo, M., et al., *The bZIP transcription factor MoAP1 mediates the oxidative stress response and is critical for pathogenicity of the rice blast fungus Magnaporthe oryzae*. PLoS Pathog, 2011. **7**(2): p. e1001302.
53. Ronen, M., S. Shalaby, and B.A. Horwitz, *Role of the transcription factor ChAP1 in cytoplasmic redox homeostasis: imaging with a genetically encoded sensor in the maize pathogen Cochliobolus heterostrophus*. Mol Plant Pathol, 2013. **14**(8): p. 786-90.
54. Segal, L.M. and R.A. Wilson, *Reactive oxygen species metabolism and plant-fungal interactions*. Fungal Genet Biol, 2018. **110**: p. 1-9.
55. Chi, M.H., et al., *A novel pathogenicity gene is required in the rice blast fungus to suppress the basal defenses of the host*. PLoS Pathog, 2009. **5**(4): p. e1000401.
56. Barbara Robbertse, O.C.Y., Anita Nguyen, Conrad L. Schoch, and B. Gillian Turgeon, *Deletion of all Cochliobolus heterostrophus Monofunctional Catalase-Encoding Genes Reveals a Role for One in Sensitivity to Oxidative Stress but None with a Role in Virulence*. Molecular Plant-Microbe Interactions, 2003. **Vol. 16**(No. 11): p. pp. 1013–1021.
57. Thordal-Christensen, H., et al., *Subcellular localization of H2O2 in plants. H2O2 accumulation in papillae and hypersensitive response during the barley—powdery mildew interaction* The Plant Journal, 2002. **11**(6): p. 1187-1194.
58. Samalova, M., et al., *Robust anti-oxidant defences in the rice blast fungus Magnaporthe oryzae confer tolerance to the host oxidative burst*. New Phytol, 2014. **201**(2): p. 556-73.
59. Huang, K., et al., *Suppression of plant-generated reactive oxygen species is required for successful infection by the rice blast fungus*. Virulence, 2011. **2**(6): p. 559-62.
60. Silva, L.V., et al., *Milbemycins: more than efflux inhibitors for fungal pathogens*. Antimicrob Agents Chemother, 2013. **57**(2): p. 873-86.
61. Bilan, D.S. and V.V. Belousov, *HyPer Family Probes: State of the Art*. Antioxid Redox Signal, 2016. **24**(13): p. 731-51.
62. Huang, K., et al., *Optimization of the HyPer sensor for robust real-time detection of hydrogen peroxide in the rice blast fungus*. Mol Plant Pathol, 2017. **18**(2): p. 298-307.
63. Poburko, D., J. Santo-Domingo, and N. Demaurex, *Dynamic regulation of the mitochondrial proton gradient during cytosolic calcium elevations*. J Biol Chem, 2011. **286**(13): p. 11672-84.

64. Mentges, M. and J. Bormann, *Real-time imaging of hydrogen peroxide dynamics in vegetative and pathogenic hyphae of Fusarium graminearum*. Sci Rep, 2015. **5**: p. 14980.
65. Bilan, D.S., et al., *HyPer-3: a genetically encoded H<sub>2</sub>O<sub>2</sub> probe with improved performance for ratiometric and fluorescence lifetime imaging*. ACS Chem Biol, 2013. **8**(3): p. 535-42.
66. Markvicheva, K.N., et al., *A genetically encoded sensor for H<sub>2</sub>O<sub>2</sub> with expanded dynamic range*. Bioorg Med Chem, 2011. **19**(3): p. 1079-84.
67. Condon, B.G.T.a.B., *Cochliobolus heterostrophus and maize: a model for genome wide integration of iron homeostasis, oxidative stress management, and virulence*.
68. Schindelin, J.A.-C., I. & Frise, E. et al., *Fiji: an open-source platform for biological-image analysis*. Nature methods, 2012. **9**: p. 676-682
69. Warner, C.A., et al., *An optical clearing technique for plant tissues allowing deep imaging and compatible with fluorescence microscopy*. Plant Physiol, 2014. **166**(4): p. 1684-7.
70. Talbot, N.J., *Having a blast: exploring the pathogenicity of Magnaporthe grisea*. Trends in Microbiology, 1995. **3**(1).
71. Dean, Y.-H.L.a.R.A., *Hydrophobicity of contact surface induces appressorium formation in Magnaporthe grisea*. FEMS Microbiology Letters, 1994. **115** p. 71-76.
72. Kankanala, P., K. Czymmek, and B. Valent, *Roles for rice membrane dynamics and plasmodesmata during biotrophic invasion by the blast fungus*. Plant Cell, 2007. **19**(2): p. 706-24.
73. G. Paul Bolwell, D.R.D., Chris Gerrish, Chung-Kyoon Auh, and Terence M. Murphy, *Comparative Biochemistry of the Oxidative Burst Produced by Rose and French Bean Cells Reveals Two Distinct Mechanisms*. Plant Physiology, 1998. **116**: p. 1379–1385.
74. Julia V. Gerasimenko, O.V.G., Altaf Palejwala, Alexei V. Tepikin, Ole H. Petersen and Alastair J. M. Watson, *Menadione-induced apoptosis: roles of cytosolic Ca<sup>2+</sup> elevations and the mitochondrial permeability transition pore*. Journal of Cell Science, 2002. **115**: p. 485-497
75. Kershaw, M.J., et al., *Magnaporthe oryzae SMO1 encodes a Ras GTPase-activating protein required for spore morphology, appressorium function and rice blast disease*. 2018.
76. M. L. Carson, C.W.S., and M. L. Senior, *Identification and Mapping of Quantitative Trait Loci Conditioning Resistance to Southern Leaf Blight of Maize Caused by Cochliobolus heterostrophus Race O*. Phytopathology, 2004. **Vol. 94**(No. 8): p. 862-867.
77. Noctor, G., A. Mhamdi, and C.H. Foyer, *Oxidative stress and antioxidative systems: recipes for successful data collection and interpretation*. Plant, Cell & Environment, 2016. **39**(5): p. 1140-1160.

78. Jelitto, T.C., *Confocal ratio imaging of cytoplasmic pH during germ tube growth and appressorium induction by Magnaporthe grisea*. *New Phytol*, 1999. **144**: p. 499–506.
79. Landraud, P., et al., *Adaptation to pH and role of PacC in the rice blast fungus Magnaporthe oryzae*. *PLoS One*, 2013. **8**(7): p. e69236.

## Appendix A

### FIJI DATA PROCESSING FOR 36 AND 48 HPI MOHYPER BARLEY INFECTION.

#### A.1 Code used for FIJI processing of MoHyPer barley infection data

```
dir1 = getDirectory("Choose Source Directory ");
dir2 = getDirectory("Choose Destination Directory ");
list = getFileList(dir1);
setBatchMode(true);
for (i=0; i<list.length; i++) {
    showProgress(i+1, list.length);
    open(dir1+list[i]);
    run("Split Channels");
    imageCalculator("Divide create 32-bit stack", "C2-"+list[i], "C1-"+list[i]);
    run("Multiply...", "value=1000 stack");
    run("Z Project...", "projection=[Max Intensity]");
    setMinAndMax(350, 2500);
    saveAs("Tiff", dir2+"MIP_"+list[i]);
    close();
}

function getFormat() {
    formats = newArray("TIFF", "dm3", "LSM", "8-bit TIFF", "JPEG", "GIF",
"PNG",
    "PGM", "BMP", "FITS", "Text Image", "ZIP", "Raw");
    Dialog.create("Batch Convert");
    Dialog.addChoice("Convert to: ", formats, "TIFF");
    Dialog.show();
    return Dialog.getChoice();
}

function convertTo8Bit() {
    if (bitDepth==24)
        run("8-bit Color", "number=256");
    else
        run("8-bit");
}
```